

Small emission sources in aggregate disproportionately account for a large majority of total methane emissions from the US oil and gas sector

James P. Williams¹, Mark Omara^{1,2}, Anthony Himmelberger², Daniel Zavala-Araiza¹, Katlyn MacKay¹, Joshua Benmergui^{1,2,3}, Maryann Sargent³, Steven C. Wofsy³, Steven P. Hamburg^{1,2}, Ritesh Gautam^{1,2}

¹Environmental Defense Fund, New York, NY, USA 10010

²MethaneSAT, LLC, Austin, TX, USA 78701

³Harvard University, Cambridge, MA, USA 02138

Correspondence to: James P. Williams (jamwilliams@edf.org), Ritesh Gautam (rgautam@edf.org)

Abstract. Reducing methane emissions from the oil and gas (oil/gas) sector has been identified as a critically important global strategy for reducing near-term climate warming. Recent measurements, especially by satellite and aerial remote sensing, underscore the importance of targeting the small number of facilities emitting methane at high rates (i.e., “super-emitters”) for measurement and mitigation. However, the contributions from individual oil/gas facilities emitting at low emission rates that are often undetected are poorly understood, especially in the context of total national- and regional-level estimates. In this work, we compile empirical measurements gathered using methods with low limits of detection to develop facility-level estimates of total methane emissions from the continental United States (CONUS) midstream and upstream oil/gas sector for 2021. We find that 70% (95% confidence intervals: 61-81%) of the total 14.6 (12.7-16.8) Tg/yr oil/gas methane emissions in the CONUS for the year 2021 originate from facilities emitting <100 kg/hr, and 30% (26-34%) and ~80% (68-90%) from facilities emitting <10 kg/hr and <200 kg/hr, respectively. While there is variability among the emission distribution curves for different oil/gas production basins, facilities with low emissions are consistently found to account for the majority of total basin emissions (i.e., range of 60% - 86% of total basin emissions from facilities emitting <100 kg/hr). We estimate that production well sites were responsible for 70% of regional oil/gas methane emissions, from which we find the well sites that accounted for only 10% of national oil and gas production in 2021, disproportionately accounted for 77% (72-81%) of the total well site emissions. Our results are also in broad agreement with data obtained from several independent aerial remote sensing campaigns (e.g., MethaneAIR, Bridger Gas Mapping LiDAR, AVIRIS-NG, and Global Airborne Observatory) across 5-8 major oil/gas basins. Our findings highlight the importance of accounting for the significant contribution of small emission sources to total oil/gas methane emissions. While reducing emissions from high-emitting facilities is important, it is not sufficient for the overall mitigation of methane emissions from the oil and gas sector which according to this study is dominated by small emission sources across the US. Tracking changes in emissions over time and designing effective mitigation policies should consider the large contribution of small methane sources to total emissions.

39 1 Introduction

40

41 Methane is a short-lived but powerful greenhouse gas with a global warming potential more than 80 times
42 stronger than carbon dioxide (CO₂) over 20 years (AR6 Synthesis Report: Climate Change 2023, 2024). Therefore,
43 the reduction of methane emissions has become a key goal to achieve rapid climate mitigation in the short term
44 (Ocko et al., 2021). In North America, one of the largest sources of methane emissions originates from the oil and
45 gas (oil/gas) sector, with most emissions originating from the production (i.e., upstream) and transportation/storage
46 (i.e., midstream) sectors (Alvarez et al., 2018). Multiple studies, especially over the past decade, have focused on the
47 quantification of methane sources from the oil/gas sector, with particular emphasis on the continental United States
48 (CONUS) (Alvarez et al., 2018; de Gouw et al., 2020; Omara et al., 2018; Lu et al., 2022; Zhang et al., 2020; Shen
49 et al., 2022; Cusworth et al., 2022; Nesser et al., 2023; Brandt et al., 2016; Duren et al., 2019; Maasackers et al.,
50 2021; Lu et al., 2023; Worden et al., 2022). Several studies have recognized the importance of a small percentage of
51 high-emitting sites (i.e. “super-emitters”) and reported them as accounting for a large fraction of total methane
52 emissions (Brandt et al., 2016; Cusworth et al., 2022; Duren et al., 2019; Sherwin et al., 2024). The emission rate
53 thresholds that characterize these super-emitting facilities are critical information for methane measurement
54 platforms, especially remote sensing technologies focused on detecting high-emitting point sources. Aerial and
55 satellite remote sensing technologies have enabled more frequent monitoring of emissions from oil and gas sites and
56 rapid mapping of large areas, although they face limitations in detection sensitivity. Despite the improved ability to
57 locate and quantify emissions from high-emitting sites, there has been considerable lack of understanding about the
58 characteristics of low methane emitting facilities, especially those emitting at rates below the limits of detection
59 (LOD) of most point-source detection remote sensing platforms, and their contributions to total oil/gas methane
60 emissions.

61 While some studies offer important yet limited insights into the contributions of different lower-emitting
62 infrastructure from the CONUS oil/gas sector, there is a lack of understanding about their overall contribution to the
63 total sectoral regional and national scale emissions. A recent study by Xia et al. (2024) combined aerial remote
64 sensing data from Bridger Gas Mapping LiDAR (Bridger GML) in four oil/gas basins supplemented with
65 component-level modeling for facilities emitting below the Bridger GML LOD and found significantly more
66 emission sources in the 1 – 10 kg/hr range when compared to the emission distribution used by the EPA (Xia et al.,
67 2024). In a study focused on production well sites in the CONUS, the main source of methane emissions from the
68 oil/gas sector (Alvarez et al., 2018; Omara et al., 2018; Rutherford et al., 2021), Omara et al. (2018) found that 90%
69 of total methane emissions from producing well sites came from those emitting at rates <100 kg/hr. A follow-up
70 study by Omara et al. (2022) highlights that the total methane emissions from low-producing well sites producing
71 less than 15 boe/day (i.e., 1 Mcf = 1,000 cubic feet of natural gas = 19.2 kg of methane at 15.6 °C and 1 atmosphere;
72 1 boe = 1 barrel of oil equivalent = 6 Mcf; assumed methane content in natural gas of 80%), which comprise 80% of

73 all producing well sites in the CONUS, were responsible for nearly half of all methane emissions from the oil/gas
74 production sector. Kunkel et al. (2023) observed that the use of the Bridger GML remote sensing platform with an
75 LOD of 3 kg/hr, combined with prior Carbon Mapper detections in a section of the Permian basin showed a
76 significant contribution from sources below the listed LOD of Carbon Mapper of 10 kg/hr. Cusworth et al. (2022)
77 found that 35% of total methane emissions (including non-oil/gas sources) from several major oil/gas producing
78 basins (other than the Appalachian basin) in the CONUS come from facilities emitting >10 kg/hr, indicating that
79 65% of emissions come from facilities emitting <10 kg/hr. Although these studies using independent measurement
80 platforms provide new emerging insights about the importance of low methane emitting oil/gas facilities, there
81 generally remains a lack of quantitative assessment of the relative fractions of emissions originating from different
82 emission rate thresholds aggregated over individual oil/gas basins as well as at a national scale.

83 There are a variety of different methane quantification methods that differ in terms of their spatial resolution of
84 sources, logistical constraints, costs of implementation, and their LODs. Measurement method sensitivities and
85 LODs have important policy implications. For example, the Environmental Protection Agency (EPA) recently
86 finalized regulations that define a “super-emitter event” as an emission rate threshold of 100 kg/hr or greater
87 (Standards of Performance for New, Reconstructed, and Modified Sources and Emissions Guidelines for Existing
88 Sources: Oil and Natural Gas Sector Climate Review, 2024), albeit without clear information on what percentage of
89 total regional emissions are captured within this definition. Satellite and aerial remote sensing methods have point
90 source LODs that range anywhere from 1-3 kg/hr for Bridger’s airborne GML (Johnson et al., 2021; Kunkel et al.,
91 2023; Thorpe et al., 2024; Xia et al., 2024) to ~200 kg/hr for GHGSat (Sherwin et al., 2023). In contrast, ground-
92 based measurement methods such as OTM-33a and tracer release have LODs <1 kg/hr (Fox et al., 2019). A study by
93 Ravikumar et al. (2018) using the Fugitive Emissions Abatement Simulation Toolkit (FEAST) suggests that a
94 method with a LOD of 0.1-1 kg/hr would sufficiently capture all emissions from the oil/gas sector, whereas the
95 ability to quantify emissions below this threshold would not lead to any significant increases in mitigation.
96 Ultimately, there is a need for clarification in the total percentage contribution of emissions originating from a given
97 emission rate threshold, which requires characterizing entire emissions distributions, not only the high emitters.

98 In this work, we create and analyze measurement-based methane emission rate distributions of US upstream and
99 midstream oil/gas facilities to determine the percentage contributions of different emission rate thresholds to total
100 methane emissions. First, we use empirical measurements gathered from ground-based sampling platforms to
101 develop a bottom-up facility-based model to estimate methane emissions for upstream and midstream facilities in
102 the continental US (CONUS) for 2021. Next, we aggregate our facility-level, population-based data to determine the
103 national- and basin-level contributions of methane emissions originating from facilities emitting at different
104 emission rate thresholds, in addition to comparisons to aerial-remote sensing platforms. Finally, we break down the
105 emission distribution curves by facility category to analyze how the percentage contributions of total emissions vary
106 across facility types.

107

108 2 Materials and methods

109

110 2.1 Empirical measurements

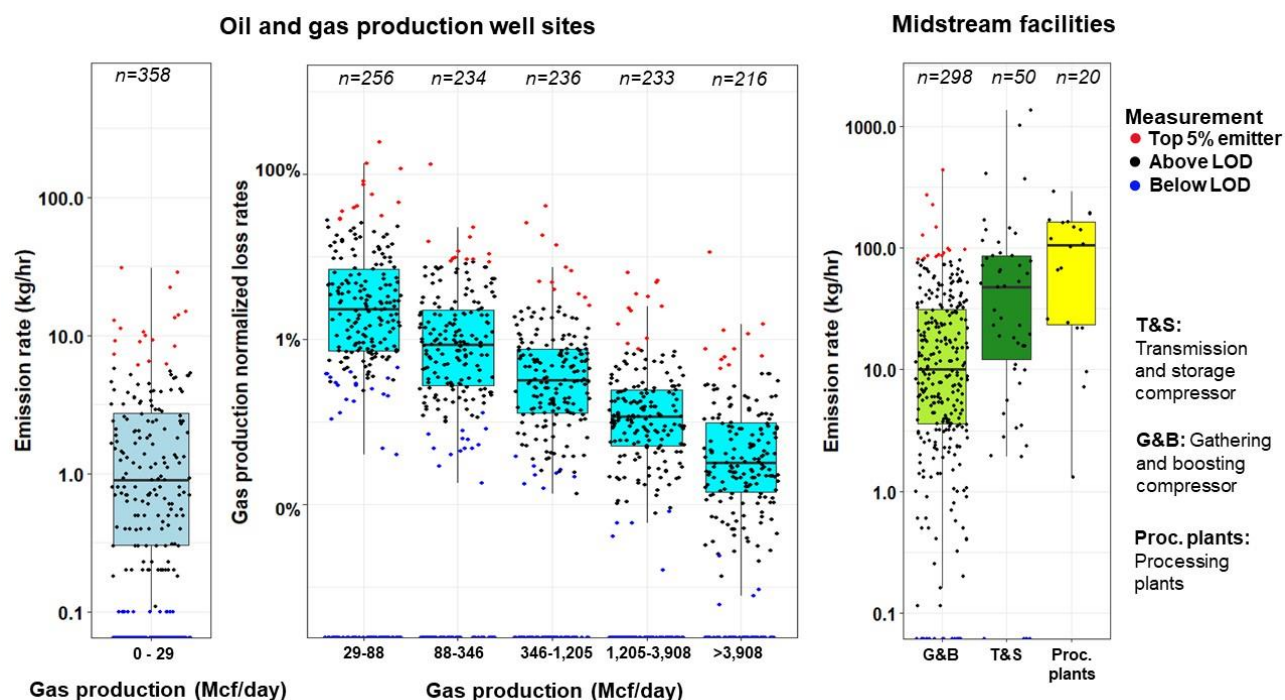
111

112 We compile 1,901 facility-level methane emission rate measurements from 16 studies (Brantley et al., 2014;
113 Caulton et al., 2019; Deighton et al., 2020; Goetz et al., 2015; Lan et al., 2015; Mitchell et al., 2015; Omara et al.,
114 2016, 2018; Rella et al., 2015; Riddick et al., 2019; Robertson et al., 2017, 2020; Subramanian et al., 2015;
115 Yacovitch et al., 2015; Zhou et al., 2021; Zimmerle et al., 2020) that use ground-based site/facility level and
116 source/component level measurement methods with low LOD's of ~0.1 kg/hr. Most (i.e., 85%) of empirical
117 measurements we use in this work were gathered using ground-based mobile laboratories that quantified methane
118 emissions at the site/facility level using either tracer-based releases, the EPA Other Test Method (OTM-33a), or
119 Gaussian plume transport modeling (Fox et al., 2019) (Table S2). The remaining 15% of empirical measurements we
120 use (Deighton et al., 2020; Riddick et al., 2019; Zimmerle et al., 2020) are ground-based methods that aggregated
121 source/component-level HiFlow sampling or static/dynamic chamber measurements, which could mean that other
122 on-site emission sources were not quantified during measurement and overall emission rate estimates are
123 conservative.

124 The compiled empirical measurements target a variety of production well sites and/or midstream facilities
125 across at least nine oil/gas-producing basins in the CONUS (Table S3). For all facility categories (i.e., production
126 well sites, gathering and boosting compressor stations, transmission and storage compressor stations, and processing
127 plants), we prioritize datasets of randomly sampled sites that include measurements below the method's LOD or
128 reported as zero emissions, except for measurements from two studies (Brantley et al., 2014; Lan et al., 2015) which
129 we discuss later in Section 2.3. Additionally, for production well site measurements, we focus only on data that
130 provide facility-level gas production data for the date/month of measurement. Our compiled dataset of
131 measurements includes both routine intentional (e.g., venting from pneumatic devices) and non-intentional (e.g.,
132 malfunctioning equipment and/or leaks from valves, connectors, flanges, etc) emissions, and while we remove any
133 measurements attributed to high emitting intermittent events such as flowbacks and liquids unloadings if that
134 information is present, we cannot fully discount that emissions from these high-emitting intermittent sources are
135 included in our compiled dataset. Furthermore, we remove any empirical measurement data associated with flaring
136 emissions, which are treated separately as discussed below, if that information is provided in the empirical data.

137 We categorize the empirical measurements by facility category as production well sites, gathering and boosting
138 compressor stations (G&B compressors), transmission and storage compressor stations (T&S compressors), or
139 processing plants. We group the empirical measurements from production well sites into six production bins based
140 on gross average daily gas production as reported in individual studies. We use gross daily average gas production
141 data instead of oil and gas production data for two reasons: 1) the limited availability of facility-level oil production
142 data provided from empirical measurement studies; and 2) the established relationship between gas production and
143 emission rates observed in previous work (Omara et al., 2018, 2022, 2024). The gas production ranges of the

144 production bins (Fig. 1) are chosen to evenly distribute empirical measurements above the method LOD to all six
 145 production bins. This categorization creates nine distinct facility categories: G&B compressors, T&S compressors,
 146 processing plants, and six groups of production well sites. We further classify the nine distinct facility categories
 147 into five primary facility categories: low-production well sites which produce combined oil and gas <15 boe/day
 148 (i.e., 0.13 kt of methane production per year), non-low-producing well sites which produce ≥ 15 boe/day, processing
 149 plants, G&B compressors, and T&S compressors. In addition to these facility categorizations, we also include
 150 Visible Infrared Imaging Radiometer Suite (VIIRS) flare detections and flared gas volume estimates in our analysis,
 151 which are treated as an independent methane source since flares can be located on multiple facility categories across
 152 the upstream and midstream oil/gas sectors.



153

154 **Figure 1:** Facility-level empirical measurement data distributed by different distinct facility categories for production well sites
 155 (left) and midstream facilities (right). Individual measurements are shown for each box plot and colored according to their
 156 emission rate status for that facility category, where blue points are considered non-detectable emissions below an emission rate
 157 threshold of ≤ 0.1 kg/hr/facility which is the method LOD we use, black points are measurements above our method LOD but
 158 below the top 5% emitter category, and red points are the top 5% of empirical emission rates for that facility category. The
 159 number of empirical measurements available for each facility category is denoted at the top of each boxplot. We show emission
 160 rates rather than loss rates for the lowest cohort of production well sites due to the reasoning presented in Section 2.3. Unit
 161 conversions: 1 Mcf = 1,000 cubic feet of natural gas = 19.2 kg of methane at 15.6 °C and 1 atmosphere; 1 boe = 1 barrel of oil
 162 equivalent = 6 Mcf; assumed methane content in natural gas of 80%.

163
 164
 165

2.2 Activity data

166 We use activity data (i.e., number of facilities and spatial locations) for actively producing wells in 2021
 167 provided by Enverus for the CONUS. We calculate both the annual averaged daily gross gas production, and oil and
 168 gas production for each producing well using the number of producing days and total annual oil and gas production

169 data provided by Enverus. We convert production wells to production well sites by spatially aggregating individual
170 wells within 25-meter (vertical wells) or 50-meter (horizontal wells) distances from each other and separately
171 merging their combined oil and gas production and gas production, and converting these production values to a mass
172 equivalent production rate in kg/hr of methane (i.e., 1 Mcf = 1,000 cubic feet of natural gas = 19.2 kg of methane at
173 15.6 °C and 1 atmosphere; 1 boe = 1 barrel of oil equivalent = 6 Mcf; assumed methane content in natural gas of
174 80%), similar to previous approaches (Omara et al., 2018).

175 We acquire activity data for operational transmission and storage (T&S) and gathering and boosting (G&B)
176 compressor stations and processing plants from Enverus for 2021 for the CONUS, which was further supplemented
177 by additional data from the Oil and Gas Infrastructure Mapping (OGIM) database published in Omara et al. (2023).
178 We filter data for these midstream facilities to include only active facilities in the year 2021. For VIIRS flare
179 detections, we use the 2021 natural gas flared volume estimates based on natural gas flaring detections provided by
180 the VIIRS instruments installed aboard satellite platforms which have a 750x750 meter source resolution (NOAA-20
181 and Suomi National Polar-orbiting Partnership) (Elvidge et al., 2015). In terms of potential double-counting between
182 the VIIRS flare detections and the empirical measurements we use in this work, the majority of VIIRS detections are
183 in the Permian, Bakken, and Eagle Ford oil/gas basins (i.e., 86% of total VIIRS detections) which corresponds to a
184 small number of our empirical measurement data (Table S3) (Plant et al., 2022). However, the limited availability of
185 spatial coordinates for our empirical measurements restricts our ability to perform a direct comparison to exclude
186 overlapping/proximal VIIRS detections and our facility-level empirical measurements. Therefore, we do
187 acknowledge that there is a possibility of double counting between our empirical measurement data and the VIIRS
188 flare detections, but we expect the degree of overlap to be low.

189 **2.3 Facility-level methane emission inventory**

190 We calculate annual methane emissions from all facility categories (i.e., six production bins of production well
191 sites, T&S compressor stations, G&B compressor stations, processing plants, and VIIRS flare detections) using a
192 multi-step probabilistic modeling approach adapted from multiple studies (Omara et al., 2018, 2022; Plant et al.,
193 2022) (Fig. 2). Briefly, for each individual facility and VIIRS flare detection in the CONUS for 2021, we estimate an
194 annually averaged methane emission rate using empirical measurement data, and consequently the cumulative
195 distribution of methane emission rates from the aggregation of these individual emission rates. Each emission rate
196 estimate is indexed according to the corresponding replicate (n=500), and we use these repetitions to determine
197 uncertainty for the cumulative methane emission distribution curves. The detailed steps of this process for all facility
198 categories and VIIRS flare detections are described below.

199 For the highest five gas production bins of producing well sites ranging from 29 to >3,908 Mcf/day (or 0.2 to
200 >27 kt of methane production per year, Figure 1), we use gross gas production normalized loss rates to model the
201 distributions used to calculate methane emission rates from Eq. (1), where the: *Loss rate* is the fraction of emitted
202 gas relative to gas production, the *emission rate* is rate of methane emitted from a facility in kilograms per hour,
203 σ_{CH_4} is the methane content of the emitted gas which we assume to be 80%, and the *gas production* is the mass

204 equivalent of natural gas produced in kilograms per hour at 1 atmosphere and 15.6 °C (1 Mcf = 1,000 cubic feet of
 205 natural gas = 19.2 kg of methane at 15.6 °C and 1 atmosphere; 1 boe = 1 barrel of oil equivalent = 6 Mcf). For the
 206 lowest well site gas production bin of 0 to 29 Mcf/day (i.e., 0 to 0.2 kt of methane production per year) and
 207 midstream facilities, we use the empirical absolute methane emission rate data as is. This approach is partly based
 208 on the methods used by Omara et al. (2022) for the low production well site category, which exploits a weak
 209 relationship between gross gas production data (which is most accessible in empirical measurement studies) and
 210 absolute emission rates to better extrapolate emissions to the entire population of production well sites in the
 211 CONUS.

$$212 \quad Loss\ rate = \frac{Emission\ rate\ \left[\frac{kg}{hr}\right]}{\sigma_{CH_4} \times Gas\ production\ \left[\frac{kg}{hr}\right]} \quad (1)$$

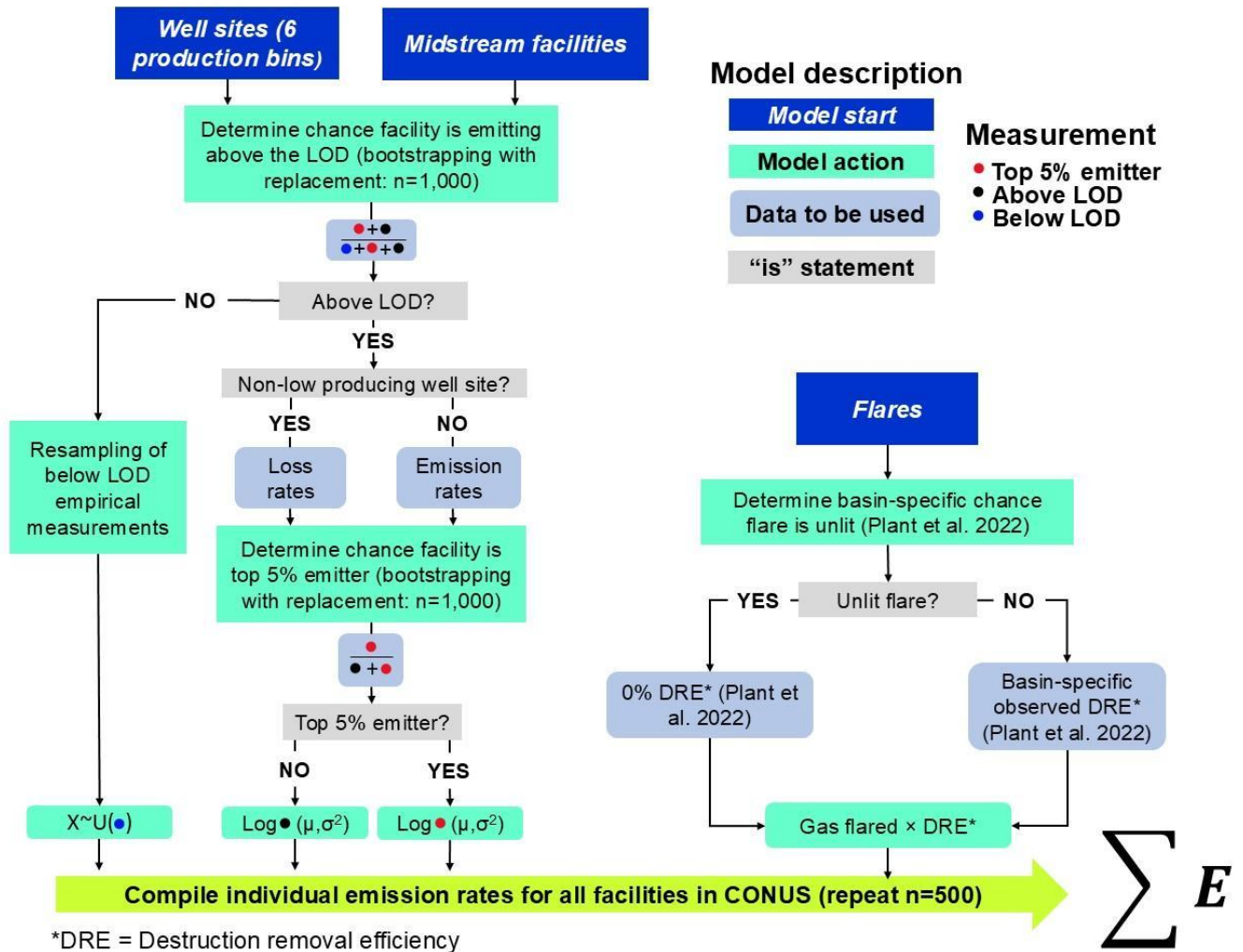
213 For our estimation of facility-level emission rates, we break down the modeling process into two separate steps:
 214 the first determines whether a randomly selected facility is emitting methane above our method LOD of ≤ 0.1
 215 kg/hr/facility, and the second determines the associated methane emission rate for that individual facility. To test the
 216 sensitivity of our method to the selection of the method LOD, we also perform an additional sensitivity analysis for
 217 other method LODs (Fig. S8). The processes outlined below are all specific to each of our nine facility categories.
 218 Brantley et al. (2014) and Lan et al. (2015) are excluded from this first step since they do not include measurements
 219 below the method LOD but include valuable data on well site emission rates with associated well site production
 220 data. To determine whether a facility is emitting methane above the method LOD threshold in our estimates, we first
 221 use bootstrapping with replacement ($n=1,000$) of our empirical measurement data to determine the chance of an
 222 individual facility emitting methane above the method LOD (i.e., ≤ 0.1 kg/hr/facility), which we call an “emitting
 223 facility” or “emitter” herein (Fig. 2). We model the results of the bootstrapping with replacement as a normal
 224 distribution and use the parameters of the modeled distribution to randomly determine whether a facility is emitting.
 225 Next, we remove the empirical measurements below the LOD and use bootstrapping with replacement ($n=1,000$) on
 226 the above LOD empirical measurements to determine the probability of an emitting facility being in the top 5% (i.e.,
 227 95th percentile or above of empirical measurement data) or bottom 95% (i.e., 95th percentile or below the empirical
 228 measurement data) of emitters, except for processing plants and T&S compressors which had too few measurements
 229 ($n=20$ and $n=50$ respectively) to distinguish between the top 5% and bottom 95% of emission or loss rates. This
 230 pseudo-random selection of a top 5% emitter within each facility category accounts for the functional definition of
 231 abnormally large emissions (i.e., super-emitters) that can be observed in all facility categories (including well sites
 232 in different production bins) (Zavala-Araiza et al. 2015, Brandt et al. 2016). We fit the results of the bootstrapping to
 233 two normal distributions: one for the top 5% of emitters and one for the bottom 95% of emitters. We use the
 234 associated parameters of each normal distribution to randomly determine whether a facility is emitting in the top 5%
 235 or bottom 95% of emitters. These steps are repeated for each facility for each facility category in the CONUS.

236 At the end of the first step of this facility-level modeling process, all facilities in the CONUS are classified as
 237 either a: bottom 95% emitter, top 5% emitter, or below the method LOD. For facilities classified as the top 5% and

238 bottom 95% of emitters, we estimate their methane emissions by first fitting a lognormal distribution to the
239 empirical measurement data, including measurements from Brantley et al. (2014) and Lan et al. (2015), of either the
240 gas production normalized loss rates or methane emission rates (Eq. 1), depending on the facility category. Next, we
241 use the parameters of the modeled distributions to randomly assign either an emission or loss rate to a randomly
242 selected facility (n=500), depending on its emitter status and facility category. We test each estimated methane
243 emission distribution to the associated empirical measurements and find a good fit for all facility categories (Table
244 S6). To account for facilities emitting below the method LOD, we randomly assign an emission rate from re-
245 sampling our dataset of empirical measurements below the method LOD for that facility category. Finally, once all
246 facilities are assigned an emission rate, we compile the ensemble of emission distributions to develop facility-level
247 emission distribution curves and total regional oil/gas methane emissions for the CONUS in 2021.

248 For all VIIRS flares detections, we use the total reported volumes of gas flared for 2021 from flares detected
249 using the VIIRS instrument (Elvidge et al. 2015) multiplied by the observed flare destruction efficiencies and
250 percentage of unlit flares from Plant et al. (2022) to calculate annual methane emission rates from this source. As
251 previously stated, our empirical measurements are largely located outside of oil/gas basins where the majority of
252 VIIRS flare detections are located (i.e. Permian, Eagle Ford, and Bakken), but we cannot discount the possibility
253 that there are instances of double-counting flares measured via our ground-based empirical data and those detected
254 by VIIRS. For each VIIRS flare detection, we randomly determine whether it is an unlit or lit flare based on the
255 basin-specific percentages of unlit flares reported by Plant et al. (2022). If a flare is determined to be lit, we use the
256 corresponding basin-specific observed destruction removal efficiencies as reported by Plant et al. (2022) multiplied
257 by the corresponding annual total volume of gas flared and convert to an emission rate. The basin-specific observed
258 destruction removal efficiencies are estimated through a fitted normal distribution using the mean and standard
259 deviations modeled from the 95% confidence intervals presented in Plant et al. (2022). If a flare is determined to be
260 unlit, we use a destruction removal efficiency of 0%. For VIIRS flare detections located outside of the Bakken,
261 Eagle Ford, and Permian basins, we used the total CONUS averaged destruction removal efficiencies of 95.2%
262 (95% confidence interval: 94.3 – 95.9%) and percentage of unlit flares of 4.1% as reported by Plant et al. (2022).

263



264

265

266

267

268

Figure 2: Flowchart describing the facility-level estimates, with steps colored according to the specific process and data being used. We note that methane emission rates for flares are calculated using a separate approach from that of production well sites and midstream facilities. Processing plants and T&S compressors are excluded from the determination of whether a facility is a top 5% emitter due to a lack of available empirical measurement data.

269

270

271

2.4 Extrapolation to smaller spatial boundaries

272

273

274

275

276

277

278

279

We perform several comparisons of our estimated emission distribution curves and total aggregated emissions to estimates from aerial and satellite remote-sensing studies. For comparisons to satellite remote-sensing studies, we prioritize national-level satellite inversions that estimate methane emissions from the CONUS that include spatially explicit maps of methane emission inversions specifically for oil/gas sources. We join the spatially explicit satellite inversions of methane emissions to the top twelve producing oil/gas basin boundaries in the CONUS, in addition to their national-level inversions which we also use for national comparisons. Since our facility-level model includes geo-located activity data (i.e., facility coordinates), we can estimate facility-level methane emissions distributions and estimate total methane emissions for any spatial boundary in the CONUS by

280 spatially joining facilities within a target boundary. Spatial variability in our facility-level estimates is driven by two
281 main factors: counts of facilities and facility types, and averaged annual production characteristics. Due to
282 constraints on data availability, we do not constrain our available empirical measurement data to the specific regions
283 where they were gathered (Table S3). We tested the sensitivity of excluding empirical measurements gathered from
284 specific oil/gas on the national emission distribution curves and total national methane emissions and found no
285 significant variation (Fig. S9). Due to a lack of data availability, we do not have sufficient spatial information from
286 empirical measurements of G&B compressors, T&S compressors, and processing plants to test for basin-level
287 differences in empirical measurement data.

288 For comparisons to aerial remote sensing studies/results, we prioritize studies that include both measured
289 point sources (i.e., oil/gas methane sources that are above the LOD of the aerial remote sensing measurement
290 platform), estimates of total regional oil/gas emissions, and descriptions/outlines of the surveyed spatial domains
291 which are required for these comparisons. Based on these criteria, we compare our estimated emissions to those
292 from peer-reviewed studies (Cusworth et al., 2022; Kunkel et al., 2023; Xia et al., 2024) and the results of research
293 flights from MethaneAIR in the Permian and Uinta oil/gas basins (Omara et al., 2024; Chan Miller et al., 2023;
294 Chulakadabba et al., 2023; MethaneAIR, 2024), with discussion in later sections on a recent study by Sherwin et al.
295 (2024). In all cases, we estimate facility-level methane emissions within the spatial domains outlined by the aerial
296 remote sensing studies to estimate region-specific methane emission distribution curves, use the relevant method
297 limits of detection to characterize emission rate thresholds valid for comparison, and subtract any emission unrelated
298 to the facility types we characterize (Chen et al., 2024). In the case of Cusworth et al. 2022, we infer the spatial
299 domains by georeferencing figures from their studies using the georeferencer tool QGIS (v.3.34.2-Prizen). We
300 compare our spatially joined facility-level emission distributions to the percentage of emissions contributed from
301 facilities emitting below discrete methane emission rate thresholds for all four aerial remote sensing studies, and to
302 the continuous cumulative methane emissions distribution curves from Bridger GML surveys (Kunkel et al., 2023;
303 Xia et al., 2024).

304 Each aerial remote sensing campaign utilizes independent methods to estimate their percentage
305 contributions from small methane sources, which in some cases requires additional analysis of the aerial remote
306 sensing results. For our analysis of continuous methane emissions distribution curves from the Bridger GML
307 campaigns (Kunkel et al., 2023; Xia et al., 2024), we restrict our analysis to estimated emission rates >3 kg/hr,
308 which is the approximate LOD of the Bridger GML remote sensing platform. For MethaneAIR, we use the
309 percentage of area emissions (i.e., diffuse area methane sources) relative to the total methane emissions for the
310 spatial boundary, which roughly corresponds to all emissions <200 kg/hr (i.e. effectively those emissions below the
311 point source detection limit of MethaneAIR that flew in multiple campaigns in the US at 40,000ft above ground
312 level (Chulakadabba et al., 2023)). MethaneAIR characterizes the total regional emissions including the spatial area
313 emissions at high resolution using a geostatistical inverse modeling framework (Miller et al., 2013) while ingesting
314 high-emitting point source information in the inversion (Chulakadabba et al., 2023; Omara et al., 2024). For
315 Cusworth et al. (2022), we analyze all campaigns by subtracting both aurally detected pipeline emissions and all

316 non-oil/gas emissions (e.g., wastewater, landfills, agriculture), since our study is focused solely on upstream and
317 midstream oil/gas sources. In addition, we subtract emissions from pipelines and non-oil/gas sources emitting below
318 aerial detection limits (i.e., TROPOMI inversions subtracted by aerially detected emissions) by estimating the
319 relative fractions of pipeline and non-oil/gas sources from the aerial detections, with the assumption that these
320 fractions are representative (Table S4). However, this process can introduce additional uncertainties in our
321 comparisons, especially for campaigns where 50% or more of aerially detected emissions were from pipelines or
322 non-oil/gas sources.

323 We account for the intermittency of detected methane sources with <3 overpasses in Cusworth et al.
324 (2022) by resampling with replacement (n=1,000) the source persistence of methane sources with ≥3 overpasses for
325 the same campaign, which is consistent with their methodology. We calculate the percentage contributions of low
326 emitting sources in Cusworth et al. (2022) using Eq. (2): where $\%E_{<x}$ is the percentage of total oil/gas methane
327 emissions below an emission rate threshold x (kg/hr), T is the total area emissions measured via TROPOMI
328 inversions (kg/hr), and $P_{>x}$ is the sum of point source emissions above the emission rate threshold x (kg/hr).

$$329 \quad \%E_{<x} = 1 - \frac{P_{>x}}{T} \quad (2)$$

330 331 **2.5 Uncertainty calculations** 332

333 Our emission distributions based on facility-level estimates incorporate uncertainty through several steps, such
334 as the: probabilistic distributions of a select facility being a top 5%, bottom 95% emitter, or facility emitting below
335 the LOD; emission rate and loss rate distributions produced from facility-level empirical measurements; and flaring
336 combustion efficiencies. In addition, we incorporate uncertainties from the empirical measurements into our facility-
337 level model by simulating new empirical emission rates based on the associated method uncertainties. At the
338 beginning of each of the 500 model iterations, we use the reported empirical methane emission rate data and
339 estimate a new emission rate using a normal distribution with the mean as the initial reported emission rate and the
340 standard deviation as a percentage of the mean value. These measurement uncertainties (i.e., 1-sigma) are chosen
341 based on the measurement methodology using the lower percentage uncertainty ranges provided by Fox et al. (2019)
342 for facilities measured via the OTM-33a (±25%), Gaussian plume dispersion (±50%), and tracer release (±20%)
343 methods. For HiFlow sampler measurements, we use an uncertainty range of ±16% (Riddick et al., 2022), and for
344 chamber-based measurements, we use ±14% (Williams et al., 2023). Therefore, each model iteration incorporates a
345 unique suite of empirical measurement data based on the initially reported emissions and their associated
346 uncertainties, which in turn impacts the probabilistic modeling of the chance of a facility emitting below the method
347 LOD, the empirical data is used to determine the parameters of the lognormal distributions of loss rates and emission
348 rates, and the ranges of the production bins. To calculate the cumulative uncertainty of our facility-level model
349 estimates, we estimate 500 methane emission distributions and aggregate the 2.5th and 97.5th percentiles of our seven
350 primary facility categories (i.e., low and non-low producing well sites, G&B compressors, T&S compressors, and

351 processing plants), which include lit and unlit VIIRS flare detection emissions, to determine our 95% confidence
352 intervals. This process is repeated for all simulations at the national-, basin-, and aerial remote sensing boundary
353 levels. For uncertainty calculations in satellite- and aerial-remote sensing studies we use for comparisons, we present
354 the reported 95% confidence intervals, if available.

355

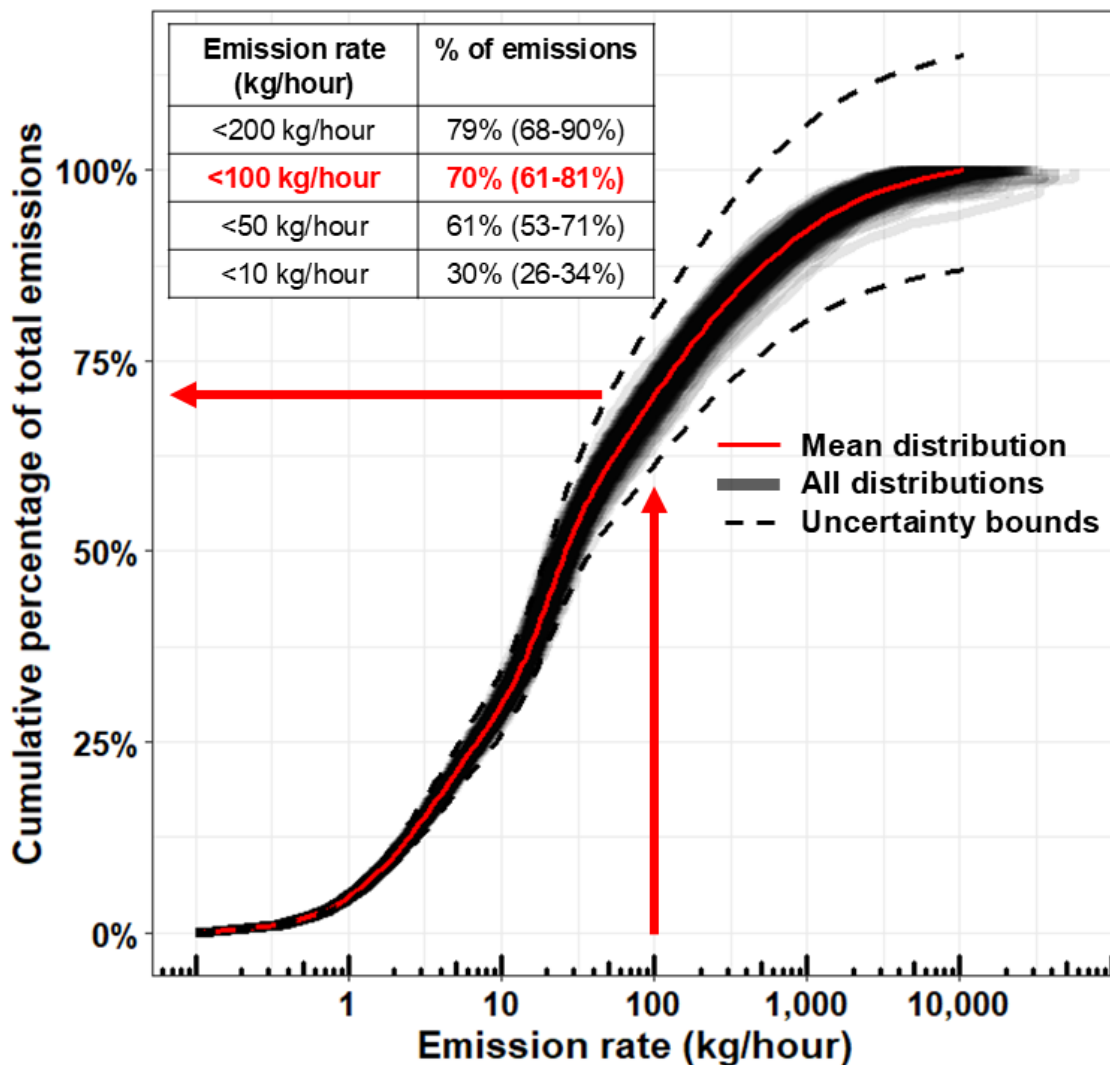
356 **3 Results**

357

358 **3.1 Distribution of emission rates at the national scale**

359

360 Based on the results from our facility-level model estimates, we estimate that 70% (95% confidence
361 interval: 61-81%) of total methane emissions from the upstream/midstream sector in the CONUS for 2021 originate
362 from facilities emitting methane at rates <100 kg/hr (Fig. 3). For other emission rate thresholds, we find that 30%
363 (26-34%) of total emissions come from facilities emitting <10 kg/hr, which corresponds to the lower thresholds of
364 aircraft-based aerial remote sensing studies (Cusworth et al., 2022; Johnson et al., 2021; Kunkel et al., 2023; Thorpe
365 et al., 2024; Xia et al., 2024), and 79% (68-90%) of total emissions come from facilities emitting <200 kg/hr. We
366 find that the emission rate threshold corresponding to 50% of cumulative methane emissions from
367 upstream/midstream facilities in the CONUS for year 2021 is 25 kg/hr (19-33 kg/hr). These results suggest that a
368 large majority of oil/gas emissions in the CONUS are not detectable by existing satellite remote-sensing point



370

371 **Figure 3:** Results from 500 estimated facility-level emission distributions showing the cumulative percentages of
 372 total methane emissions contributed from facilities emitting below methane emission rate thresholds. For example,
 373 facilities emitting <100 kg/hr account for 70% (61-81%) of total methane emissions. The inset table in the upper left
 374 displays the total percentage of methane emissions contributed from several discrete emission rate thresholds with
 375 95% confidence intervals shown in parenthesis.

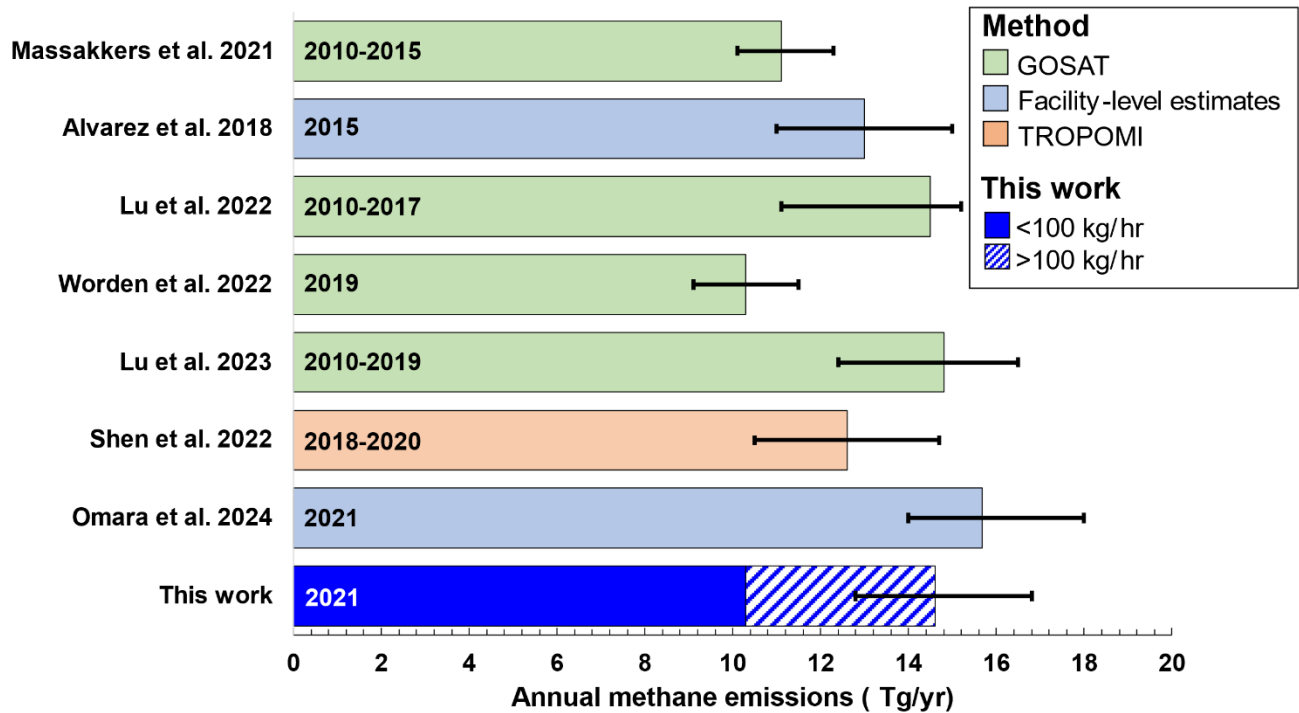
376

377 The distribution for our national-level methane emissions follows an S-shaped curve, noting that the x-axis
 378 (i.e., facility-level methane emission rates) is presented in the log₁₀ scale. From 0.1 to 1 kg/hr, we observe a plateau
 379 in the distribution curve indicating that increasing emission rates within this range do not significantly increase the
 380 percentage contribution to total regional emissions (Fig. 3), similar to the findings in Ravikumar et al. (2019). From 1
 381 to 100 kg/hr, we see a sharper rise in the emission distribution, indicating that increasing emission rates at this range
 382 lead to a more substantial contribution to total methane emissions, and account for 68% (60 – 75%) of total methane

383 emissions (Fig. 3, Table S4). Above an emission rate threshold of 100 kg/hr, we see an exponential decline in the
384 percentage contributions of total emission with increasing emission rates, with total methane emissions in this range
385 amounting to 28% (18 – 37%) of the total oil/gas emissions. Facilities emitting at the 1-10 kg/hr and 100-1,000 kg/hr
386 ranges contribute a similar cumulative percentage at 26% (23 - 29%) and 22% (18 - 26%) respectively. Similar
387 percentage contributions are also observed between the 0.1-1 kg/hr and >1,000 kg/hr ranges at 4.5% (4.0 - 5.1%) and
388 6.1% (2.6 - 13%) respectively. Overall, we find that the highest contribution to total national CONUS methane
389 emissions occurs from facilities emitting in the 10-100 kg/hr range at 42% (37 - 46%). In terms of facility counts,
390 from the 673,940 total active oil/gas facilities we estimate in the CONUS for 2021, we estimate that essentially all
391 (i.e., ~99.9%) of these facilities emit methane below 100 kg/hr.

392 Our facility-level model estimates total methane emissions from US upstream/midstream oil/gas emissions
393 for 2021 to be 14.6 (12.7 - 16.8) Tg/yr, or 1,668,000 (1,453,000 – 1,921,000) kg/hr (Fig. 4), which corresponds to a
394 gross gas production normalized loss rate of 2.4%, assuming a uniform 80% methane content in natural gas across
395 oil/gas producing regions in the CONUS. This national emission total of 14.6 (12.7 - 16.8) Tg/yr is more than
396 double the EPA Greenhouse Gas Inventory Report for natural gas and petroleum systems in 2021, excluding post-
397 meter and distribution methane emissions (Inventory of U.S. Greenhouse Gas Emissions and Sinks, 2024). We
398 compare our total national estimates to previous estimates by seven studies that predominantly utilize satellite-based
399 remote-sensing platforms such as GOSAT and TROPOMI inversions (Lu et al., 2022, 2023; Maasackers et al.,
400 2021; Shen et al., 2022; Worden et al., 2022) except for Alvarez et al. (2018) and Omara et al. (2024) who developed
401 unique facility-based modeling approaches using empirical measurement data collected from multiple oil/gas basins
402 in the CONUS (Fig. 4). Our estimate of national methane emissions overlaps with six out of seven other national
403 estimates of oil/gas methane emissions for the US, with a combined average of 13.1 (ranging from 11.1 - 15.7)
404 Tg/yr. We do not estimate methane emissions from gathering/transmission/distribution pipelines, post-meter
405 emissions, abandoned oil and gas wells, and refineries due to the scarcity of measurement-based data for these
406 sources. Total methane emissions from these sources emit ~2 Tg/year of methane emissions based on other studies
407 (Williams et al., 2021; Alvarez et al., 2018; Omara et al., 2024; Weller et al., 2020; Inventory of U.S. Greenhouse
408 Gas Emissions and Sinks, 2024). Overall, our total national estimate of CONUS methane emissions for 2021 shows

409 good agreement with multiple independent and recent measurement-based estimates.



410

411 **Figure 4:** Comparison of total CONUS oil/gas emissions for 2021 from this facility-level measurement-based
412 inventory compared to empirical estimates from other studies. Bars are colored according to the methodology used
413 to derive the total national estimates, and the years within the bars represent the corresponding time periods for the
414 estimates. Black inset lines represent 95% confidence intervals. Our total estimates for “This work” do not include
415 emissions from other oil/gas methane sources such as abandoned oil and gas wells,
416 transmission/gathering/distribution pipelines, post-meter emissions, and refineries. Emission estimates from Omara
417 et al. (2024) do not include methane emissions from abandoned oil and gas wells. We assume that the remote
418 sensing estimates (i.e., GOSAT and TROPOMI) include all oil/gas methane sources, including downstream
419 emissions.

420

421 3.2 Distribution of emission rates at the basin-level scale

422

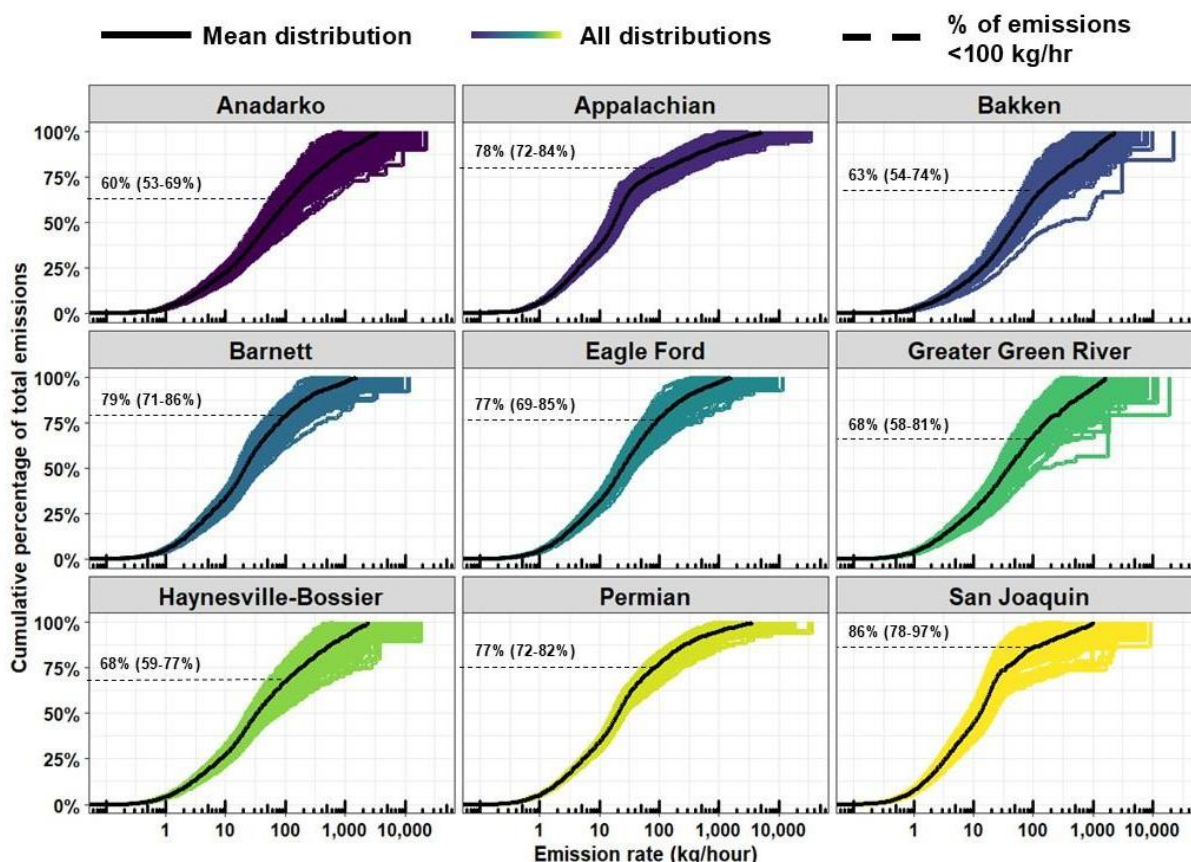
423 Among the top nine emitting oil/gas basins in the CONUS, we observe variations among the different
424 basins in terms of the methane emission distributions, especially at higher emission rate thresholds (Fig. 5). The
425 majority of the top nine emitting oil/gas basins in Fig. 5 show higher percentage contributions from facilities
426 emitting <100 kg/hr when compared to our national estimate of 70% (61 – 81%) (Fig. 3). These percentage
427 contributions vary from ~80% in the Permian, Appalachian, and Eagle Ford basins, up to ~90% in the oil-dominant
428 San Joaquin basin. Only the Anadarko and Bakken basins have notably lower contributions to total emissions at the
429 100 kg/hr threshold at ~60% compared to the national level, which is still a significant majority of total methane
430 emissions. Despite these variations, our facility-level model estimates that the majority of total national oil/gas
431 emissions are consistently contributed from facilities emitting <100 kg/hr for the top nine emitting basins.

432 Our estimated facility-level emission distributions for the top nine emitting oil/gas basins all follow an S-
433 shaped curve (Fig. 5) like the national distribution (Fig. 3), albeit with certain variations. For all basins, the initial
434 plateau in the emissions distribution curves ends at around 1 kg/hr before beginning to rise more steeply. For the
435 Appalachian and San Joaquin basins, the second plateau is at the 20-50 kg/hr emission rate threshold (Fig. 5). For
436 the remaining basins, the rise in the emission distribution curves plateaus gradually, indicating a more consistent
437 relationship of emission rate thresholds to their contribution to total emissions. The variability displayed among the
438 500 basin-level simulations differs among the oil/gas basins, with less spread in the 500 estimated methane
439 emissions distributions for the Appalachian, Anadarko, and Permian basins compared to the Uinta, Denver-
440 Julesburg, and San Joaquin basins (Fig. 5 and Fig. S6). These variations are likely caused in part by the overall total
441 basin-level methane emissions, where an extremely high estimated methane emission rate would have a greater
442 impact on the percentage contribution to the total for basins with lower overall emissions (e.g., the apparent outliers
443 for the Greater Green River and Bakken basins in Fig. 5). We discuss below other plausible causes for basin-to-
444 basin variability in the estimated methane emission distributions.

445 In terms of total methane emissions, the top two emitting oil/gas basins are the Permian and Appalachian,
446 which collectively account for 5.2 (4.4 – 6.3) Tg/year (Fig. S1) or 37% of total upstream and midstream oil/gas
447 methane emissions. This exceeds the cumulative contribution from the other seven highest emitting oil/gas basins
448 which collectively account for 3.7 (2.9 – 5.0) Tg/yr. Notably, we find that the highest emissions in the CONUS
449 occur from regions outside of any basin boundary 4.3 (1.2 – 6.3) Tg/year. Our estimates for basin-level total
450 emissions also show good agreement with remote-sensing satellite-based observations (Fig. S1), except for the
451 Appalachian, Bakken, Greater Green River, and Denver-Julesburg basins where our results are consistently more
452 than double those from the remote-sensing studies that used a prior-emission based inversion result (Lu et al., 2023;
453 Shen et al., 2022). These four basins are in regions with relatively low TROPOMI observation counts and densities
454 compared to other regions in the CONUS (Shen et al., 2022), in addition to other factors that could influence
455 satellite-based inversions such as the presence of many non-oil/gas sources such as coal, livestock, and landfills.
456 Overall, our estimates of total basin-level emissions are consistent with satellite-based observations.

457

458



459

460 **Figure 5:** A) Results from 500 model simulations showing the cumulative methane emissions distribution curves for
 461 total upstream/midstream oil/gas methane emissions for the top nine emitting oil/gas basins in the CONUS for 2021.
 462 The model averages for each basin are shown in solid black lines. Inset dashed lines represent the percentage
 463 contributions of total emission from sources emitting <100 kg/hr. Emission distribution curves for the remaining
 464 eleven oil/gas basins in the CONUS are shown in Fig. S6, and a map of the spatial boundaries used for the different
 465 oil/gas basins is shown in Fig. S10.

466

467 3.3 Distribution of emission rates by facility category

468

469 We find significant variations in the methane emission rate distribution curves among the different facility
 470 categories (Fig. 6A). Over 50% of total methane emissions from low (i.e., <15 boe/day, or <0.13 kt of methane
 471 production per year and non-low production well sites, lit flares, and G&B compressor stations occur from facilities
 472 emitting <100 kg/hr (Fig. 6A). In contrast, only 17% (15-18%) of emissions from processing plants, 19% (18-20%)
 473 of emissions from T&S compressor stations, and 9% (7-12%) of emissions from unlit flares are contributed from
 474 emission sources <100 kg/hr. Similar variability is also observed at other emission rate thresholds, such as only 1%
 475 (0-2%) of total emissions for T&S compressor stations, unlit flares, and processing plants originating from facilities
 476 emitting at rates <10 kg/hr, compared to 50% (43-58%) from low producing well sites and 30% (24-35%) from non-
 477 low producing well sites (Fig. 6A). At higher emission rate thresholds, we find that 33% (20-45%) of total emissions
 478 from T&S compressors and processing plants are emitted from facilities <200 kg/hr, compared to 84% (68-93%)

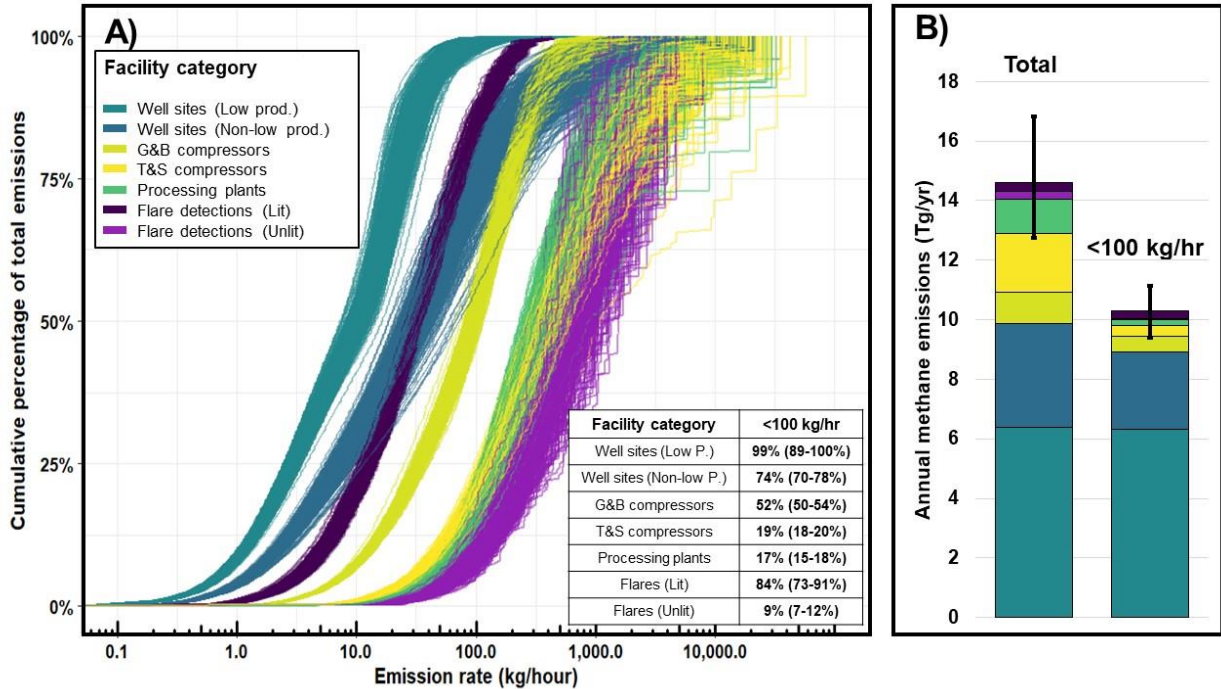
479 from non-low producing well sites (>boe/day of combined oil and gas), 86% (83-88%) from VIIRS flare detections,
480 78% (70-86%) from G&B compressor stations, and essentially 100% of emissions from low producing well sites.

481 A breakdown of the 673,940 total facilities in our model has 541,970 as low-producing well sites, followed
482 by 121,824 non-low-production well sites, 4,431 G&B compressor stations 2,093 T&S compressor stations, 919
483 processing plants, and 3,153 total VIIRS flare detections. Of these 673,940 total facilities, 99.5% (99.4 – 99.6%)
484 emit methane at rates <100 kg/hr (Fig. S11), and in turn contribute 70% of total methane emissions (Fig. 3). Overall,
485 we estimate that 68% of total CONUS oil/gas methane emissions for 2021 come from production well sites, of
486 which 44% are from low-production well sites with combined oil/gas production <15 boe/day (i.e., <0.13 kt of
487 methane production per year) , and the remaining 24% from non-low production well sites (i.e., >15 boe/day) (Fig.
488 6B). Midstream facilities contribute 29% of total methane emissions, with 13% from T&S compressors, 8% from
489 processing plants, 7% from G&B compressor stations. The remaining 4% from VIIRS flare detections are evenly
490 split with 2% each from lit and unlit flares respectively. Based on the population counts for each facility category
491 and their corresponding total methane emissions, the average methane emission rate per facility category is highest
492 for processing plants at 146 (115 – 283) kg/hr, followed by 106 (89 – 129) kg/hr for T&S compressor stations, 27
493 (25 - 29) kg/hr for G&B compressor stations, 3.3 (2.9 – 3.8) kg/hr for non-low producing well sites, and 1.3 (1.2 –
494 1.5) kg/hr for low producing well sites. For VIIRS flares detections, we find a large difference in average emissions
495 between lit flares at 11 (9.2 – 13) kg/hr and unlit flares at 205 (132 – 294) kg/hr.

496 Production well sites constitute the bulk of total methane emissions among the facility categories we
497 considered, with most of these emissions contributed from low production well sites. Overall, we find that 77% (72-
498 81%) of well site emissions originated from only 10% of national oil and gas production in 2021 (Fig. S7),
499 highlighting a disproportionately large fraction of emissions relative to production. In terms of individual well site
500 level production values, the same 77% (72-81%) of total cumulative methane emissions were contributed from well
501 sites producing >50 boe/day (i.e., 0.43 kt of methane production per year) or lower. For well sites producing 15
502 boe/day (i.e., 0.13 kt of methane production per year) or lower, which is the production threshold used to define a
503 well site as being marginally producing in previous work (Deighton et al., 2020; Omara et al., 2022), we find that
504 these low producing well sites accounted for 65% (58-69%) of total well site emissions, or 6.4 Tg/yr (4.7-6.8 Tg/yr).

505

506



507

508 **Figure 6:** A) Results from an ensemble of 500 estimated methane emission distributions showing the percentage of
 509 total methane emissions among facility categories contributed from facilities emitting at rates below an emission rate
 510 threshold. The inset table on the bottom right displays the discrete percentage contributions to total methane
 511 emissions contributed from facilities emitting <100 kg/hr. B) Breakdown of total annual methane emissions
 512 contributed from all emitting facility categories and those emitting at rates <100 kg/hr.

513

514 3.4 Comparisons to aerial remote sensing studies

515

516 We perform comparisons of the percentage contributions of methane emissions from facilities emitting
 517 below discrete emission rate thresholds between seven aerial remote sensing campaigns across four distinct regions
 518 and our estimated facility-level results (Fig. 7). The aerial remote sensing technologies include data from Bridger
 519 GML measurements (Kunkel et al., 2023; Xia et al., 2024), MethaneAIR (Omara et al. 2024; Miller et al. 2023), and
 520 the results from Global Airborne Observatory and next-generation Airborne Visible/Infrared Imaging Spectrometer
 521 campaigns (Cusworth et al., 2022) which are also included in the aerial detections used by Sherwin et al. (2024). In
 522 comparing the percentage contributions to total emissions from low-emitting sources between our facility-level
 523 estimates and the aerial remote sensing campaigns, we find that emission contributions agree well across aerial
 524 remote sensing campaigns for the total percentage of methane emissions from facilities emitting, as seen in Fig. 7
 525 for both less than 100 kg/hr and 200 kg/hr.

526 For the Bridger GML remote sensing campaigns (Kunkel et al., 2023; Xia et al., 2024), we find good
 527 agreement in the percentage of total emissions contributed from facilities emitting <200 and <100 kg/hr compared to
 528 our facility-level model estimates (Fig. 7). A comparison of continuous emissions distribution curves between our

529 facility-level emission distributions and two Bridger GML aerial remote sensing campaigns (Kunkel et al., 2023;
530 Xia et al., 2024) targeting four oil/gas basins is shown in Fig. S3. The Bridger GML aerial sampling platform has the
531 lowest LOD among the aerial campaigns we analyze in this work and a similar source resolution (i.e., 30 meters) to
532 our facility-level model (i.e., 50 meters), allowing for a more detailed comparison of continuous emission
533 distribution curves due to the higher number of detected methane sources at low emission rates provided by Bridger
534 GML surveys. We find close agreement between our facility-level methane emission distribution curves and the
535 observed emissions by Bridger GML in the four-basin aggregate provided by Xia et al. (2024) (Fig. S3A) which
536 includes Anadarko, Bakken, Eagle Ford and Permian basins (individual basin data are not currently available in Xia
537 et al. (2024)), as well as separately for the Permian remote sampling campaign (Fig. S3B) by Kunkel et al. (2023),
538 with the measured emissions from the Bridger GML surveys overlapping with our facility-level model simulations
539 throughout the continuous distribution of methane emission rates.

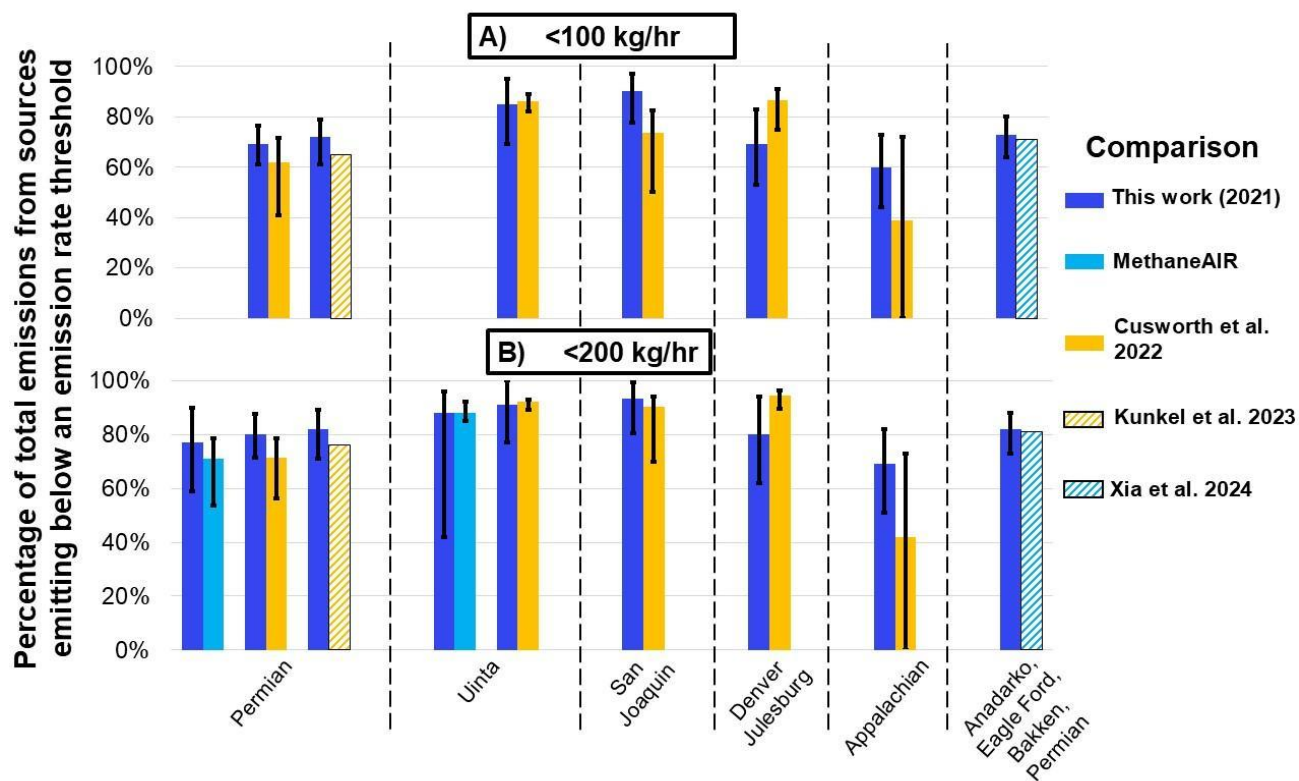
540 For the multiple aerial remote sensing campaigns performed by Cusworth et al. (2022), we generally find
541 good agreement with all of our estimates statistically overlapping for discrete emissions rate thresholds of <100
542 kg/hr and <200 kg/hr for the Permian and Uinta oil/gas basins (Fig. 7). For the San Joaquin and Denver-Julesburg
543 oil/gas basins, we see good agreement at the emission rate threshold of <200 kg/hr and at <100 kg/hr (i.e.
544 overlapping uncertainty bounds). For the Appalachian basin, we find broad agreement at both emission rate
545 thresholds of <100 kg/hr and <200 kg/hr, with our results consistently showing a 20-30% greater contribution from
546 emission sources below the discrete emission rate thresholds (Fig. 7). We find the closest agreement in the Permian
547 and Uinta oil/basins, where the differences in the average percentage contributions vary from -9% to +4% across the
548 three discrete emission rate thresholds of <100 and <200 kg/hr (Fig. 7). In Denver-Julesburg and Appalachian
549 basins, the differences are observed to be larger, compared to other basins, where the differences in average
550 percentage contributions across the discrete emission thresholds vary from -30% to +18%, however, they are within
551 our estimated uncertainty bounds. The detected point sources by Cusworth et al. (2022) in the Denver-Julesburg and
552 Appalachian basins contain many non-oil/gas point sources (Table S4), which may lead to additional uncertainty in
553 the comparisons for these basins since we use the relative proportions of point sources to subtract an estimated
554 contribution of non-oil/gas point sources from the TROPOMI estimates to provide a more direct comparison
555 between our estimates (since our study only focuses on upstream and midstream oil and gas sectors) and those of
556 Cusworth et al. (2022). Notably, the Appalachian basin contains the highest percentage contribution of non-oil/gas
557 point sources at 67% (Table S4). In contrast, we note that all of the detected point sources by Cusworth et al. (2022)
558 in the Permian and Uinta basins were attributed to oil/gas point sources (Table S4).

559 Our comparisons to the available flight results from MethaneAIR, which quantifies both total regional
560 methane emissions and high-emitting point sources >200 kg/hr from the same aerial platform (Chulakadabba et al.,
561 2023), show close agreement between our facility-level estimates and the available aerial campaigns in the Uinta
562 and Permian basins for facilities emitting <200 kg/hr (Fig. 7B). For the MethaneAIR flight in the Uinta basin, we
563 estimate that 92% (46 - 100%) of total oil/gas methane emissions are from sources emitting <200 kg/hr, compared to
564 88% from MethaneAIR (Fig. 7B). For the available flight in the Permian basin from MethaneAIR, we estimate total

565 contributions from sources emitting <200 kg/hr at 77% (59 – 90%) compared to the 71% estimated by MethaneAIR
 566 (Fig. 7B).

567 Overall, our findings show that our facility-level estimates closely agree with the results from multiple
 568 aerial remote sensing campaigns from different regions and using various measurement methods.

569



570
 571 **Figure 7:** Comparisons of the cumulative percentage of oil/gas methane emissions from all oil/gas facilities emitting
 572 A) <100 kg/hr, and B) <200 kg/hr, between our facility-level empirical emissions estimates and aerial remote
 573 sensing campaigns. Bars are colored according to the study and grouped according to the target oil/gas basin(s). All
 574 results from the facility-level simulations (i.e., this work) are constrained to the spatial boundaries of the aerial
 575 campaigns for direct comparisons (note that for a given basin, spatial boundaries might be slightly different).
 576 Uncertainty bars for the facility-level simulations are the 2.5th and 97.5th percentiles of 500 simulations. Maps of all
 577 spatial boundaries used for comparisons are provided in Fig. S2. Comparisons to MethaneAIR are not performed at
 578 the <100 kg/hr threshold because MethaneAIR detections are not available for point sources below this emission
 579 rate threshold.

580

581 **4 Discussion**

582

583 Understanding how facilities with different magnitudes of emissions contribute to total regional emissions
584 has direct policy implications for methane quantification and mitigation, such as the selection of
585 measurement/screening methods with the appropriate detection sensitivities (Ravikumar et al., 2018). Our main
586 finding is that 70% of total oil/gas methane emissions from the upstream/midstream sectors come from facilities
587 emitting at rates <100 kg/hr, which is the emission rate threshold above which point source emissions are referred
588 to as “super-emitting” oil/gas source by the EPA (Standards of Performance for New, Reconstructed, and Modified
589 Sources and Emissions Guidelines for Existing Sources: Oil and Natural Gas Sector Climate Review, 2024). While
590 detecting and mitigating emissions from super emitters are important (Cusworth et al., 2022; Duren et al., 2019;
591 Sherwin et al., 2024), our results underscore the need to account for oil/gas methane sources emitting at lower rates,
592 as the cumulative contribution of lower-emitting sites accounts for a large majority of emissions across US oil/gas
593 basins. Facility-level, measurement-based data collected in other countries present a similar story. From a sample of
594 sites (n=302) measured via Bridger GML remote sensing platform in British Columbia, Canada (Tyner and Johnson,
595 2021), roughly 60% of the total quantified oil/gas site-level emissions originate from sites emitting <32 kg/hr. In
596 Romania, a site-level measurement-based inventory (Stavropoulou et al., 2023) using 178 measurements finds that
597 oil production facilities emitting <100 kg/hr contribute 78% of total oil/gas methane emissions in the studied region.
598 In short, the high percentage contribution from lower-emitting (<100 kg/hr) oil/gas facilities that account for a large
599 majority of total emissions is not unique to the US and is likely present in other countries as well. A combination of
600 approaches that characterize entire emission distributions across populations of sites (i.e., not just focusing on
601 measuring super-emitters) and quantification of regional-level emissions is needed in other countries to quantify the
602 relative contributions of low-emitting sources that in aggregate can be significant sources of overall oil/gas methane
603 emissions. Most of our analysis centers around quantifying the percentage contributions of oil/gas methane sources
604 emitting below one discrete emission rate threshold (i.e., <100 kg/hr, per EPA’s definition of a super-emitter). We
605 estimate that over 99% of the total oil/gas facilities that we analyze in this work emit below 100 kg/hr (Fig. S11),
606 which in turn contribute 70% (61 – 81%) of total methane emissions (Fig. 3). The emission rate threshold of 100
607 kg/hr is relevant to US policy decisions (EPA’s Final Rule for Oil and Natural Gas Operations Will Sharply Reduce
608 Methane and Other Harmful Pollution., 2024), but we also illustrate the importance of a complete characterization of
609 emissions, which gains importance as newer methane monitoring technologies have different LODs. For example,
610 the effective LOD at high probabilities of detection for available point source imaging satellites of ~200 kg/hr
611 (Jacob et al., 2022) would only be able to quantify 21% (10-32%) of all oil/gas point sources in the CONUS, if the
612 full oil/gas sector was mapped in its entirety, based on our facility-level results. When considering the relationship
613 of facility-level emission rates to total cumulative methane emissions, we find that oil/gas methane emissions in the
614 CONUS are dominated by many low-emitting facilities, which relates directly to methane measurement
615 technologies.

616 Point source-focused remote sensing platforms offer the advantage of rapidly surveying large areas (i.e.,
617 100’s-1,000’s km²) which facilitates the detection and quantification of high-emitting point sources (Cusworth et al.,
618 2022; Duren et al., 2019; Sherwin et al., 2024). In contrast, logistical constraints often limit the sample sizes for
619 ground-based vehicle sampling platforms, however, these limitations can be overcome with stratified random,

620 representative sampling and statistical analysis approaches like this work. Ground-based measurement platforms
621 provide much lower LODs (i.e., <1 kg/hr) when compared to remote sensing platforms, which are necessary to
622 quantify emissions from the large number of small methane sources we find that contribute roughly three-quarters of
623 total regional oil/gas emissions in the CONUS and will only improve as additional ground-based measurements are
624 gathered. Overall, our main findings highlight the importance of methods that can rapidly locate the small number of
625 high-emitting point sources we estimate, but our findings emphasize the need to account for the disproportionately
626 large majority percentage of total regional oil/gas emissions that are emitted from smaller diffuse methane sources.

627 When extrapolating our facility-level model results to the basin-level we see variations among the emission
628 distribution curves for different oil/gas basins, but still find that most methane emissions come from facilities
629 emitting <100 kg/hr. The variations in the emission distribution curves for different basins are driven by many
630 factors, such as the: production characteristics, number and density of facilities, different types and relative counts of
631 facility categories, the availability of empirical measurement data used to model emissions, and the total oil/gas
632 methane emissions (i.e., the denominator). For example, the Appalachian basin is dominated by a high number of
633 older low-production well sites (Deighton et al., 2020; Riddick et al., 2019; Enverus, 2024) with fewer midstream
634 facilities such as processing plants and G&B compressors, which contrasts with the Bakken basin where we find a
635 high number of midstream facilities, high-producing well sites, and VIIRS flare detections (Elvidge et al., 2015;
636 Enverus, 2024). When comparing the emissions distribution curves for the Bakken and Appalachian basins (Fig. 5),
637 we observe higher contributions from lower-emitting facilities for the Appalachian compared to the Bakken. An
638 example of differences in basin-level production is shown in Fig. S4 and Fig. S5, where we see variable profiles
639 among the different oil and gas-producing basins in terms of well site production characteristics, which are the main
640 source of total methane emissions in this work (Fig. 6). We also observe the influence of total basin-level emissions
641 on the variability among our emission distribution curves, where large emitting sources in the San Joaquin basin can
642 lead to high variability among the estimated emission distribution curves compared to the Permian basin which has
643 roughly ten times the total emissions compared to the San Joaquin (Fig. 5). We note that a direct comparison of our
644 model results with aerial remote sensing methods may be limited, in part, by methodological differences in methane
645 quantification approaches (and underlying uncertainties). The remote sensing observations assessed here as
646 snapshots may capture facility-level emission distributions that are not well represented in annually averaged
647 methane emissions distributions, as we estimate here. Nevertheless, we find broad agreement with these independent
648 aerial remote sensing estimates at the basin scale and across smaller spatial domains, as discussed. Ultimately, as
649 many characteristics will influence methane emissions distribution curves among different oil/gas producing regions
650 in the CONUS, mitigation strategies will need to be structured accordingly to the region they are targeting.

651 Our results find that over half of cumulative methane emissions from three different facility categories
652 come from facilities emitting <100 kg/hr, including methane emissions from lit and unlit flares. We show how the
653 large contributions from small methane sources to total regional emissions are not unique to any one facility
654 category, but it is important to contextualize our emission distribution curves with the corresponding total regional
655 emissions. Our facility-level estimates find that the main source of oil/gas methane emissions in the CONUS are

656 oil/gas production well sites, of which the low production category is responsible for 44% (39 – 49%) of the total
657 estimated oil/gas methane emissions in the CONUS in 2021. Low-producing well sites, also known as “marginal
658 wells”, have been shown in previous work to be a significant source of methane emissions, especially relative to
659 their contribution to overall oil/gas production (Deighton et al., 2020; Omara et al., 2022). Omara et al. (2022) found
660 that marginal wells contributed anywhere from 37%-75% of total methane emissions from production well sites,
661 which is like our estimates (i.e., 65%). Despite low production well sites having a lower mean emission rate
662 compared to other facility categories, the large facility counts result in significant aggregate total emissions of
663 methane. This implies that detection and mitigation strategies to reduce methane emissions from these and other
664 low-emitting oil and gas infrastructure (e.g., abandoned oil/gas wells) would require alternative mitigation and
665 detection approaches compared to those for the small number of super-emitting emission sources. For detection,
666 measurement methods that can measure emission rates between 0.1-100 kg/hr are required, since this range makes
667 up 70% of total methane emissions (Figure 3 and Table S1) as modeled herein. In terms of methane mitigation
668 policy, financial incentives, like the USD 4.7 billion from the Biden Bipartisan Infrastructure Law for abandoned
669 wells, could be used to prioritize the repair of old and leak-prone production well sites, as these low-producing well
670 sites only account for a small fraction (i.e., 5.6% in 2019) of total oil/gas production (Omara et al., 2022).

671 We see good agreement between our facility-level results and a majority of aerial remote sensing studies, which
672 are expected to capture a wide range of high-emitting facilities in a survey region. For example, when comparing
673 our model results to Kunkel et al. (2023) and Xia et al. (2024) we find that our estimated methane emissions closely
674 match the distribution of methane emissions measured in Bridger GML surveys (Fig. S3). We also find good
675 agreement to satellite remote sensing estimates of emissions, such as our basin-level (Fig. S1) and national-level
676 comparison to satellite inversions (Fig. 3), and other aerial remote sensing study regions (Table S2). Our
677 comparisons of the contributions of low-emitting sources below discrete emission rate thresholds also agree closely
678 with recent MethaneAIR, Kairos Aerospace, GAO, and AVIRIS-NG aerial surveys, whose results also highlight the
679 importance of small methane sources to overall oil/gas methane emissions. Recently, Sherwin et al. (2024)
680 suggested that a majority of total emissions originate from a small fraction of high-emitting sites. Notably, most of
681 the aerial measurements that are used in Sherwin et al. (2024) are obtained from the Cusworth et al. (2022) study,
682 with which we see good agreement (Fig. 7). Sherwin et al. (2024) perform an alternative analysis than Cusworth et
683 al. (2022) for aeri ally measured sources with <3 overpasses and assume that sources with one or two overpasses
684 emit at their observed intermittency of 100%, 50%, or 0% of the time. This difference in analytical approaches
685 produces higher contributions from aerial emissions in Sherwin et al. (2024) by 31% on average for seven aerial
686 campaigns compared to Cusworth et al. (2022) (Table S7), which uses a resampling approach described earlier in
687 the Methods Section 2.4. In addition, emissions from Sherwin et al. (2024) that are below aerial detection limits are
688 estimated using a combination of an equipment-level bottom-up model presented in Rutherford et al. (2021) for
689 production well sites, and emission factors from the U.S. Greenhouse Gas Inventory (Inventory of U.S. Greenhouse
690 Gas Emissions and Sinks, 2024) for midstream facilities, which produces 52% lower emissions on average for seven
691 aerial campaigns (Table S7). Therefore, the aeri ally measured emissions in Sherwin et al. (2024) are higher and the
692 emissions below aerial detection limits are lower which leads to a higher contribution to total methane emissions

693 from high-emitting facilities (Table S7). Ultimately, the broad agreement we find across multiple disparate
694 measurement techniques and platforms across Bridger GML aerial campaigns (Kunkel et al., 2023; Xia et al., 2024),
695 MethaneAIR measurements (MethaneAIR L4 Area Sources 2021 | Earth Engine Data Catalog, 2024; Omara et al.,
696 2024), and the multiple surveyed regions presented in Cusworth et al. (2022), altogether provide collective evidence
697 about the large contribution of smaller emission sources to total regional emissions.

698 Given the variability in methane detection technologies, a range of approaches can be taken to estimate methane
699 emission rate distributions, each providing unique advantages and disadvantages. MethaneAIR provides a novel
700 remote sensing approach where high-emitting point sources, distributed area sources and total regional emissions are
701 quantified using the same aerial platform, providing the ability to directly measure high-emitting point source and
702 diffuse area contributions to total regional estimates. In the work by Xia et al. (2024) they combine measurements
703 from Bridger GML across four oil/gas basins and use component-level simulations to account for facilities emitting
704 below the 3 kg/hr LOD of Bridger GML. Other approaches also exist, such as Cusworth et al. (2022) who combine
705 TROPOMI inversions to estimate total regional methane emissions with point source emissions quantified from their
706 aerial detection platforms (i.e., GAO, AVIRIS-NG). Similarly, Sherwin et al. (2024) combine point source emissions
707 measured via aerial remote sensing with site/facility-level emission rates estimates calculated from a combination of
708 an equipment-level bottom-up model for production well sites (Rutherford et al., 2021) and emission factors from the
709 2023 GHGI for midstream facilities (Inventory of U.S. Greenhouse Gas Emissions and Sinks, 2024) for facilities
710 emitting below aerial detection limits. Remote sensing studies have key advantages over ground-based sampling
711 platforms, such as rapidly surveying wide areas and capturing higher-emitting point sources, but have variable LODs
712 depending on the target region, topography, measurement technology, presence of co-located non-oil/gas methane
713 sources (i.e., source attribution), weather conditions, infrastructure density, and infrastructure type(s). These variables
714 pose additional challenges when quantifying the contributions from facilities emitting above/below specific emission
715 rate thresholds, which are critical information to inform mitigation policy. Assessing performance, tracking mitigation,
716 and accurate reporting requires building a comprehensive picture of emissions by characterizing all emitters big and
717 small, and reconciling with total basin/sub-basin level emissions. Ultimately, the key seems to be merging the best
718 data from both approaches to build a hybrid inventory, ideally using a multi-tiered system with multiple methods that
719 span a range of LODs that allow for gathering empirical measurements from facilities emitting at all parts of the
720 methane emission distribution curve. Our study is a step in that direction considering measurement-based data while
721 presenting a robust comparison with available independent remote sensing measurements. At the same time, large-
722 area aggregate emissions data obtained from wide-area remote sensing mapping or mass balance surveys can better
723 constrain total regional emissions (e.g. Cusworth et al. 2022; Omara et al. 2024) towards a more empirically robust
724 denominator in characterizing the relative contributions of small emission and high emission sources to total
725 emissions.

726 We show that our facility-level emission models produce national- and basin-level methane emissions estimates
727 that are in good agreement with other independent measurement-based studies. However, we note the following
728 limitations/biases that could be improved with future data collection efforts. The empirical measurements that we

729 use in our model are representative of the year and time they were measured (i.e., 2010-2020), meaning that they
730 would not reflect any updates in regulatory practices or changes in facility operational and emission management
731 practices. In addition, there are variations in the number of production well site empirical measurements among
732 oil/gas basins (Table S3) although a sensitivity analysis shows that excluding data from individual oil/gas basins
733 does not significantly impact our results (Fig. S9). Furthermore, there are several oil/gas methane emission sources
734 that we do not account for in our estimates, which include: gathering/transmission/distribution pipelines, oil refining
735 and transportation, abandoned oil/gas wells, offshore oil/gas infrastructure, post-meter sources, and oil/gas
736 distribution infrastructure in urban areas. For some sources omitted in this work such as abandoned oil/gas wells,
737 their inclusion would likely lead to a higher contribution from low-emitting facilities, since the highest recorded
738 emission rate from an abandoned oil/gas well is 76 kg/hr (Riddick et al., 2024). For others such as oil refineries,
739 their inclusion would likely lead to a lower contribution from small methane sources given their low facility counts
740 and high per-site emissions (Duren et al., 2019). Despite their omissions, total methane emissions from these sources
741 are currently estimated to account for 5-10% (Alvarez et al., 2018; Riddick et al., 2024; Inventory of U.S.
742 Greenhouse Gas Emissions and Sinks, 2024; Williams et al., 2021) of total oil/gas sectoral emissions. Our estimates
743 also utilize empirically measured emission rates from ground-based sampling platforms which are limited in
744 number, especially in the case of processing plants (n=20) and T&S compressor stations (n=50) (Table S2). The
745 empirical data used in our analysis includes a smaller sample of super-emitting facilities relative to those captured
746 by remote sensing platforms (Duren et al., 2019; Sherwin et al., 2024), but our use of production-normalized loss
747 rates and lognormal distributions to estimate facility-level methane emission rates anticipates and accounts for the
748 possibility of finding low-probability, high-magnitude emissions that occur at rates beyond those that appear in our
749 dataset of empirical observations. For example, our highest empirical emission rate is 1,360 kg/hr for a T&S
750 compressor station, whereas our maximum estimated facility-level emission rate across all 500 facility-level
751 emission distribution curves averages 7,500 kg/hr (3,000 - 21,000 kg/hr). Finally, we include a small number (i.e.,
752 5% of total empirical data used in the model) of measurements for production well-sites gathered using ground-
753 based component/source-level sampling methods from two studies (Deighton et al., 2020; Riddick et al., 2019). All
754 measurements from these two studies targeted the lowest production cohort of production well sites and exhibited
755 statistically lower emission rates than those gathered using facility-level ground-based methods for the same well
756 site production cohort, meaning that any bias introduced by the inclusion of these measurements would lead towards
757 the underestimation of total emissions and/or the percentage contributions from low-emitting sources. Despite these
758 limitations, we have shown that our results are broadly in agreement with satellite- and aerial-based remote sensing
759 studies at national/basin/local scales, and other facility-level estimates.

760 Going forward, several approaches can be used to better understand the percentage contributions from facilities
761 emitting at different leak rate thresholds, and ultimately improve our understanding of oil/gas methane emissions in
762 the CONUS and around the world. A combination of multiple satellite and aerial remote sensing approaches and
763 synthesis of their data by bringing in point source detections at multiple thresholds at the same time characterizing
764 total regional emissions as demonstrated using a compilation of multi-scale measurements seems a viable pathway
765 towards building a more complete picture of the overall methane emissions. Combining aerial and satellite remote

766 sensing measurements with ground-based site/facility-level estimates presents itself as an effective next step, as
767 implemented/suggested by prior studies (Allen, 2014; Alvarez et al., 2018). Aerial or satellite remote sensing
768 platforms focused on point source detection offer the ability to rapidly locate the small number of the highest
769 emitting facilities that contribute a disproportionate fraction of emissions, offering valuable data on specific facility
770 locations that allow for rapid mitigation. However, more direct observational approaches are needed to acquire total
771 emissions data which according to this study is dominated by small-emitting sources that are undetected by high-
772 emitting point source detection systems. Facility-level population-based approaches can account for the lower-
773 emitting facilities that contribute the most total oil/gas methane emissions, which is needed for accurate emission
774 reporting and understanding the contributions of total emissions above/below emission rate thresholds. The ground-
775 based estimates can be further constrained by large-area aggregated emission quantification provided by regional
776 remote sensing or mass balance mapping approaches (Shen et al., 2022; Omara et al., 2024; Jacob et al., 2022)
777 towards producing a more robust overall emission quantification.

778 **5 Conclusions**

779 In conclusion, our work highlights several key aspects of oil/gas methane emission rate distribution curves
780 in the CONUS for 2021, which include:

- 781 1. A large majority (70%) of total national continental oil/gas methane emissions in the US originate from
782 lower-emitting facilities (<100 kg/hr).
- 783 2. Emission rate distributions vary among different oil/gas basins, but among the top nine producing basins
784 we consistently find that most methane emissions (60%-86%) originate from oil/gas facilities emitting at
785 rates <100 kg/hr.
- 786 3. Production well sites were found to be responsible for 70% of regional oil/gas methane emissions, from
787 which the sites that accounted for only 10% of national oil and gas production in 2021, disproportionately
788 accounted for 77% (72-81%) of the total well site emissions.
- 789 4. Our results were consistently found to be in close agreement with those from independent aerial/satellite
790 remote sensing estimates, both in comparing contributions from discrete emission rate thresholds and
791 continuous emissions distribution curves, which emphasize the importance of the large majority
792 contribution of small-emitting methane sources to total oil/gas methane emissions.

793 Our results highlight, and quantify, the significant contributions of the large number of low-emitting oil/gas
794 facilities to total regional/basin/local oil/gas methane emissions in the CONUS for 2021. In addition to the CONUS,
795 the small oil/gas methane sources are likely a significant component of total regional emissions in other countries as
796 well as recent data suggest from Romania and Canada (Stavropoulou et al., 2023; Tyner and Johnson, 2021) and
797 would need to be further investigated to build a comprehensive assessment of small-emitting methane emissions and
798 their relative contributions to total oil/gas methane emissions globally. This work emphasizes the need for multi-

799 scale approaches to quantify total regional oil/gas methane emissions; and at the same time characterize and account
800 for the large contribution from small emission sources dispersed across a wide area, in addition to incorporating data
801 on high-emitting point sources towards producing overall robust methane emission quantification.

802
803 **Data availability**

804 All 500 full emission rate distributions at the national level are available to download from Zenodo (link:
805 <https://doi.org/10.5281/zenodo.13314532>). All estimated methane emission rate distributions at the basin or small
806 target scale are available upon request. Empirical measurement data used in the estimation of the methane emission
807 distribution curves are available from the references listed in Table S2.

808
809 **Code availability**

810 R code used to create the methane emission distribution curves and figures is available upon reasonable request.

811
812 **Acknowledgements**

813 We acknowledge funding support from the Bezos Earth Fund. We would like to thank Jack Warren for his valuable
814 efforts in analyzing point source emissions from MethaneAIR aerial campaigns.

815
816 **Author contributions**

817 JPW and RG designed this study. JPW created the code used to produce all results, with inputs from MO, KM, DZA,
818 and AH. MethaneAIR analysis was provided by JB, MS, and SW. Multi-sensor airborne intercomparison was
819 performed by JPW and RG. JPW prepared the manuscript with input from all co-authors.

820
821 **Competing interests**

822 The authors declare that they have no conflict of interest.

823
824 **References**

825 Allen, D. T.: Methane emissions from natural gas production and use: reconciling bottom-up and top-down
826 measurements, *Current Opinion in Chemical Engineering*, 5, 78–83, <https://doi.org/10.1016/j.coche.2014.05.004>,
827 2014.

828 Alvarez, R. A., Zavala-Araiza, D., Lyon, D. R., Allen, D. T., Barkley, Z. R., Brandt, A. R., Davis, K. J., Herndon, S.
829 C., Jacob, D. J., Karion, A., Kort, E. A., Lamb, B. K., Lauvaux, T., Maasackers, J. D., Marchese, A. J., Omara, M.,
830 Pacala, S. W., Peischl, J., Robinson, A. L., Shepson, P. B., Sweeney, C., Townsend-Small, A., Wofsy, S. C., and
831 Hamburg, S. P.: Assessment of methane emissions from the U.S. oil and gas supply chain, *Science*, 361, 186–188,
832 <https://doi.org/10.1126/science.aar7204>, 2018.

- 833 Enverus | Creating the future of energy together.: <https://www.enverus.com/>, last access: 25 March 2024.
- 834 Standards of Performance for New, Reconstructed, and Modified Sources and Emissions Guidelines for Existing
835 Sources: Oil and Natural Gas Sector Climate Review: <https://www.federalregister.gov/documents/2024/03/08/2024-00366/standards-of-performance-for-new-reconstructed-and-modified-sources-and-emissions-guidelines-for>, last
836 access: 22 July 2024.
- 837
- 838 AR6 Synthesis Report: Climate Change 2023: <https://www.ipcc.ch/report/ar6/syr/>, last access: 6 March 2024.
- 839 MethaneAIR L4 Area Sources 2021 | Earth Engine Data Catalog: [https://developers.google.com/earth-
840 engine/datasets/catalog/EDF_MethaneSAT_MethaneAIR_methaneair-L4area-2021](https://developers.google.com/earth-engine/datasets/catalog/EDF_MethaneSAT_MethaneAIR_methaneair-L4area-2021), last access: 27 March 2024.
- 841 Brandt, A. R., Heath, G. A., and Cooley, D.: Methane Leaks from Natural Gas Systems Follow Extreme Distributions,
842 *Environ. Sci. Technol.*, 50, 12512–12520, <https://doi.org/10.1021/acs.est.6b04303>, 2016.
- 843 Brantley, H. L., Thoma, E. D., Squier, W. C., Guven, B. B., and Lyon, D.: Assessment of Methane Emissions from
844 Oil and Gas Production Pads using Mobile Measurements, *Environ. Sci. Technol.*, 48, 14508–14515,
845 <https://doi.org/10.1021/es503070q>, 2014.
- 846 Caulton, D. R., Lu, J. M., Lane, H. M., Buchholz, B., Fitts, J. P., Golston, L. M., Guo, X., Li, Q., McSpirtt, J., Pan,
847 D., Wendt, L., Bou-Zeid, E., and Zondlo, M. A.: Importance of Superemitter Natural Gas Well Pads in the Marcellus
848 Shale, *Environ. Sci. Technol.*, 53, 4747–4754, <https://doi.org/10.1021/acs.est.8b06965>, 2019.
- 849 Chan Miller, C., Roche, S., Wilzewski, J. S., Liu, X., Chance, K., Souri, A. H., Conway, E., Luo, B., Samra, J.,
850 Hawthorne, J., Sun, K., Staebell, C., Chulakadabba, A., Sargent, M., Benmergui, J. S., Franklin, J. E., Daube, B. C.,
851 Li, Y., Laughner, J. L., Baier, B. C., Gautam, R., Omara, M., and Wofsy, S. C.: Methane retrieval from MethaneAIR
852 using the CO₂ Proxy Approach: A demonstration for the upcoming MethaneSAT mission, *EGUsphere*, 1–40,
853 <https://doi.org/10.5194/egusphere-2023-1962>, 2023.
- 854 Chen, Y., Sherwin, E. D., Berman, E. S. F., Jones, B. B., Gordon, M. P., Wetherley, E. B., Kort, E. A., and Brandt, A.
855 R.: Quantifying Regional Methane Emissions in the New Mexico Permian Basin with a Comprehensive Aerial Survey,
856 *Environ. Sci. Technol.*, 56, 4317–4323, <https://doi.org/10.1021/acs.est.1c06458>, 2022.
- 857 Chen, Y., Sherwin, E. D., Wetherley, E. B., Yakovlev, P. V., Berman, E. S. F., Jones, B. B., Hmiel, B., Lyon, D. R.,
858 Duren, R., Cusworth, D. H., and Brandt, A. R.: Reconciling ultra-emitter detections from two aerial hyperspectral
859 imaging surveys in the Permian Basin, 2024.
- 860 Chulakadabba, A., Sargent, M., Lauvaux, T., Benmergui, J. S., Franklin, J. E., Chan Miller, C., Wilzewski, J. S.,
861 Roche, S., Conway, E., Souri, A. H., Sun, K., Luo, B., Hawthorne, J., Samra, J., Daube, B. C., Liu, X., Chance, K.,
862 Li, Y., Gautam, R., Omara, M., Rutherford, J. S., Sherwin, E. D., Brandt, A., and Wofsy, S. C.: Methane point source
863 quantification using MethaneAIR: a new airborne imaging spectrometer, *Atmospheric Measurement Techniques*, 16,
864 5771–5785, <https://doi.org/10.5194/amt-16-5771-2023>, 2023.
- 865 Cusworth, D. H., Thorpe, A. K., Ayasse, A. K., Stepp, D., Heckler, J., Asner, G. P., Miller, C. E., Yadav, V., Chapman,
866 J. W., Eastwood, M. L., Green, R. O., Hmiel, B., Lyon, D. R., and Duren, R. M.: Strong methane point sources
867 contribute a disproportionate fraction of total emissions across multiple basins in the United States, *Proceedings of
868 the National Academy of Sciences*, 119, e2202338119, <https://doi.org/10.1073/pnas.2202338119>, 2022.
- 869 Deighton, J. A., Townsend-Small, A., Sturmer, S. J., Hoschouer, J., and Heldman, L.: Measurements show that
870 marginal wells are a disproportionate source of methane relative to production, *Journal of the Air & Waste
871 Management Association*, 70, 1030–1042, <https://doi.org/10.1080/10962247.2020.1808115>, 2020.
- 872 Duren, R. M., Thorpe, A. K., Foster, K. T., Rafiq, T., Hopkins, F. M., Yadav, V., Bue, B. D., Thompson, D. R.,
873 Conley, S., Colombi, N. K., Frankenberg, C., McCubbin, I. B., Eastwood, M. L., Falk, M., Herner, J. D., Croes, B. E.,
874 Green, R. O., and Miller, C. E.: California’s methane super-emitters, *Nature*, 575, 180–184,
875 <https://doi.org/10.1038/s41586-019-1720-3>, 2019.

- 876 Elvidge, C. D., Zhizhin, M., Baugh, K., Hsu, F.-C., and Ghosh, T.: Methods for Global Survey of Natural Gas Flaring
877 from Visible Infrared Imaging Radiometer Suite Data, *Energies*, 9, 14, <https://doi.org/10.3390/en9010014>, 2015.
- 878 Fox, T. A., Barchyn, T. E., Risk, D., Ravikumar, A. P., and Hugenholtz, C. H.: A review of close-range and screening
879 technologies for mitigating fugitive methane emissions in upstream oil and gas, *Environ. Res. Lett.*, 14, 053002,
880 <https://doi.org/10.1088/1748-9326/ab0cc3>, 2019.
- 881 Goetz, J. D., Floerchinger, C., Fortner, E. C., Wormhoudt, J., Massoli, P., Knighton, W. B., Herndon, S. C., Kolb, C.
882 E., Knipping, E., Shaw, S. L., and DeCarlo, P. F.: Atmospheric Emission Characterization of Marcellus Shale Natural
883 Gas Development Sites, *Environ. Sci. Technol.*, 49, 7012–7020, <https://doi.org/10.1021/acs.est.5b00452>, 2015.
- 884 de Gouw, J. A., Veefkind, J. P., Roosenbrand, E., Dix, B., Lin, J. C., Landgraf, J., and Levelt, P. F.: Daily Satellite
885 Observations of Methane from Oil and Gas Production Regions in the United States, *Sci Rep*, 10, 1379,
886 <https://doi.org/10.1038/s41598-020-57678-4>, 2020.
- 887 Jacob, D. J., Varon, D. J., Cusworth, D. H., Dennison, P. E., Frankenberg, C., Gautam, R., Guanter, L., Kelley, J.,
888 McKeever, J., Ott, L. E., Poulter, B., Qu, Z., Thorpe, A. K., Worden, J. R., and Duren, R. M.: Quantifying methane
889 emissions from the global scale down to point sources using satellite observations of atmospheric methane,
890 *Atmospheric Chemistry and Physics*, 22, 9617–9646, <https://doi.org/10.5194/acp-22-9617-2022>, 2022.
- 891 Johnson, M. R., Tyner, D. R., and Szekeres, A. J.: Blinded evaluation of airborne methane source detection using
892 Bridger Photonics LiDAR, *Remote Sensing of Environment*, 259, 112418, <https://doi.org/10.1016/j.rse.2021.112418>,
893 2021.
- 894 Kunkel, W. M., Carre-Burritt, A. E., Aivazian, G. S., Snow, N. C., Harris, J. T., Mueller, T. S., Roos, P. A., and
895 Thorpe, M. J.: Extension of Methane Emission Rate Distribution for Permian Basin Oil and Gas Production
896 Infrastructure by Aerial LiDAR, *Environ. Sci. Technol.*, 57, 12234–12241, <https://doi.org/10.1021/acs.est.3c00229>,
897 2023.
- 898 Lan, X., Talbot, R., Laine, P., and Torres, A.: Characterizing Fugitive Methane Emissions in the Barnett Shale Area
899 Using a Mobile Laboratory, *Environ. Sci. Technol.*, 49, 8139–8146, <https://doi.org/10.1021/es5063055>, 2015.
- 900 Lu, X., Jacob, D. J., Wang, H., Maasackers, J. D., Zhang, Y., Scarpelli, T. R., Shen, L., Qu, Z., Sulprizio, M. P.,
901 Nesser, H., Bloom, A. A., Ma, S., Worden, J. R., Fan, S., Parker, R. J., Boesch, H., Gautam, R., Gordon, D., Moran,
902 M. D., Reuland, F., Villasana, C. A. O., and Andrews, A.: Methane emissions in the United States, Canada, and
903 Mexico: evaluation of national methane emission inventories and 2010–2017 sectoral trends by inverse analysis of in
904 situ (GLOBALVIEWplus CH₄ ObsPack) and satellite (GOSAT) atmospheric observations, *Atmospheric Chemistry
905 and Physics*, 22, 395–418, <https://doi.org/10.5194/acp-22-395-2022>, 2022.
- 906 Lu, X., Jacob, D. J., Zhang, Y., Shen, L., Sulprizio, M. P., Maasackers, J. D., Varon, D. J., Qu, Z., Chen, Z., Hmiel,
907 B., Parker, R. J., Boesch, H., Wang, H., He, C., and Fan, S.: Observation-derived 2010-2019 trends in methane
908 emissions and intensities from US oil and gas fields tied to activity metrics, *Proceedings of the National Academy of
909 Sciences*, 120, e2217900120, <https://doi.org/10.1073/pnas.2217900120>, 2023.
- 910 Maasackers, J. D., Jacob, D. J., Sulprizio, M. P., Scarpelli, T. R., Nesser, H., Sheng, J., Zhang, Y., Lu, X., Bloom, A.
911 A., Bowman, K. W., Worden, J. R., and Parker, R. J.: 2010–2015 North American methane emissions, sectoral
912 contributions, and trends: a high-resolution inversion of GOSAT observations of atmospheric methane, *Atmospheric
913 Chemistry and Physics*, 21, 4339–4356, <https://doi.org/10.5194/acp-21-4339-2021>, 2021.
- 914 Miller, S. M., Wofsy, S. C., Michalak, A. M., Kort, E. A., Andrews, A. E., Biraud, S. C., Dlugokencky, E. J.,
915 Eluszkiewicz, J., Fischer, M. L., Janssens-Maenhout, G., Miller, B. R., Miller, J. B., Montzka, S. A., Nehrkorn, T.,
916 and Sweeney, C.: Anthropogenic emissions of methane in the United States, *Proceedings of the National Academy of
917 Sciences*, 110, 20018–20022, <https://doi.org/10.1073/pnas.1314392110>, 2013.
- 918 Mitchell, A. L., Tkacik, D. S., Roscioli, J. R., Herndon, S. C., Yacovitch, T. I., Martinez, D. M., Vaughn, T. L.,
919 Williams, L. L., Sullivan, M. R., Floerchinger, C., Omara, M., Subramanian, R., Zimmerle, D., Marchese, A. J., and

- 920 Robinson, A. L.: Measurements of Methane Emissions from Natural Gas Gathering Facilities and Processing Plants:
921 Measurement Results, *Environ. Sci. Technol.*, 49, 3219–3227, <https://doi.org/10.1021/es5052809>, 2015.
- 922 Nesser, H., Jacob, D. J., Maasackers, J. D., Lorente, A., Chen, Z., Lu, X., Shen, L., Qu, Z., Sulprizio, M. P., Winter,
923 M., Ma, S., Bloom, A. A., Worden, J. R., Stavins, R. N., and Randles, C. A.: High-resolution U.S. methane emissions
924 inferred from an inversion of 2019 TROPOMI satellite data: contributions from individual states, urban areas, and
925 landfills, *EGUsphere*, 1–36, <https://doi.org/10.5194/egusphere-2023-946>, 2023.
- 926 Ocko, I. B., Sun, T., Shindell, D., Oppenheimer, M., Hristov, A. N., Pacala, S. W., Mauzerall, D. L., Xu, Y., and
927 Hamburg, S. P.: Acting rapidly to deploy readily available methane mitigation measures by sector can immediately
928 slow global warming, *Environ. Res. Lett.*, 16, 054042, <https://doi.org/10.1088/1748-9326/abf9c8>, 2021.
- 929 Omara, M., Sullivan, M. R., Li, X., Subramanian, R., Robinson, A. L., and Presto, A. A.: Methane Emissions from
930 Conventional and Unconventional Natural Gas Production Sites in the Marcellus Shale Basin, *Environ. Sci. Technol.*,
931 50, 2099–2107, <https://doi.org/10.1021/acs.est.5b05503>, 2016.
- 932 Omara, M., Zimmerman, N., Sullivan, M. R., Li, X., Ellis, A., Cesa, R., Subramanian, R., Presto, A. A., and Robinson,
933 A. L.: Methane Emissions from Natural Gas Production Sites in the United States: Data Synthesis and National
934 Estimate, *Environ. Sci. Technol.*, 52, 12915–12925, <https://doi.org/10.1021/acs.est.8b03535>, 2018.
- 935 Omara, M., Zavala-Araiza, D., Lyon, D. R., Hmiel, B., Roberts, K. A., and Hamburg, S. P.: Methane emissions from
936 US low production oil and natural gas well sites, *Nat Commun*, 13, 2085, <https://doi.org/10.1038/s41467-022-29709-3>, 2022.
- 938 Omara, M., Himmelberger, A., MacKay, K., Williams, J. P., Benmergui, J., Sargent, M., Wofsy, S. C., and Gautam,
939 R.: Constructing a measurement-based spatially explicit inventory of US oil and gas methane emissions, *Earth System
940 Science Data Discussions*, 1–25, <https://doi.org/10.5194/essd-2024-72>, 2024.
- 941 Plant, G., Kort, E. A., Brandt, A. R., Chen, Y., Fordice, G., Gorchov Negron, A. M., Schwietzke, S., Smith, M., and
942 Zavala-Araiza, D.: Inefficient and unlit natural gas flares both emit large quantities of methane, *Science*, 377, 1566–
943 1571, <https://doi.org/10.1126/science.abq0385>, 2022.
- 944 Ravikumar, A. P., Wang, J., McGuire, M., Bell, C. S., Zimmerle, D., and Brandt, A. R.: “Good versus Good Enough?”
945 Empirical Tests of Methane Leak Detection Sensitivity of a Commercial Infrared Camera, *Environ. Sci. Technol.*, 52,
946 2368–2374, <https://doi.org/10.1021/acs.est.7b04945>, 2018.
- 947 Rella, C. W., Hoffnagle, J., He, Y., and Tajima, S.: Local- and regional-scale measurements of CH₄, δ¹³CH₄, and C₂H₆
948 in the Uintah Basin using a mobile stable isotope analyzer, *Atmospheric Measurement Techniques*, 8, 4539–4559,
949 <https://doi.org/10.5194/amt-8-4539-2015>, 2015.
- 950 Riddick, S. N., Mauzerall, D. L., Celia, M. A., Kang, M., Bressler, K., Chu, C., and Gum, C. D.: Measuring methane
951 emissions from abandoned and active oil and gas wells in West Virginia, *Science of The Total Environment*, 651,
952 1849–1856, <https://doi.org/10.1016/j.scitotenv.2018.10.082>, 2019.
- 953 Riddick, S. N., Ancona, R., Mbua, M., Bell, C. S., Duggan, A., Vaughn, T. L., Bennett, K., and Zimmerle, D. J.: A
954 quantitative comparison of methods used to measure smaller methane emissions typically observed from
955 superannated oil and gas infrastructure, *Atmospheric Measurement Techniques*, 15, 6285–6296,
956 <https://doi.org/10.5194/amt-15-6285-2022>, 2022.
- 957 Riddick, S. N., Mbua, M., Santos, A., Emerson, E. W., Cheptonui, F., Houlihan, C., Hodshire, A. L., Anand, A.,
958 Hartzell, W., and Zimmerle, D. J.: Methane emissions from abandoned oil and gas wells in Colorado, *Science of The
959 Total Environment*, 922, 170990, <https://doi.org/10.1016/j.scitotenv.2024.170990>, 2024.
- 960 Robertson, A. M., Edie, R., Snare, D., Soltis, J., Field, R. A., Burkhart, M. D., Bell, C. S., Zimmerle, D., and Murphy,
961 S. M.: Variation in Methane Emission Rates from Well Pads in Four Oil and Gas Basins with Contrasting Production
962 Volumes and Compositions, *Environ. Sci. Technol.*, 51, 8832–8840, <https://doi.org/10.1021/acs.est.7b00571>, 2017.

- 963 Robertson, A. M., Edie, R., Field, R. A., Lyon, D., McVay, R., Omara, M., Zavala-Araiza, D., and Murphy, S. M.:
 964 New Mexico Permian Basin Measured Well Pad Methane Emissions Are a Factor of 5–9 Times Higher Than U.S.
 965 EPA Estimates, *Environ. Sci. Technol.*, 54, 13926–13934, <https://doi.org/10.1021/acs.est.0c02927>, 2020.
- 966 Rutherford, J. S., Sherwin, E. D., Ravikumar, A. P., Heath, G. A., Englander, J., Cooley, D., Lyon, D., Omara, M.,
 967 Langfitt, Q., and Brandt, A. R.: Closing the methane gap in US oil and natural gas production emissions inventories,
 968 *Nat Commun*, 12, 4715, <https://doi.org/10.1038/s41467-021-25017-4>, 2021.
- 969 Shen, L., Gautam, R., Omara, M., Zavala-Araiza, D., Maasakkers, J. D., Scarpelli, T. R., Lorente, A., Lyon, D., Sheng,
 970 J., Varon, D. J., Nesser, H., Qu, Z., Lu, X., Sulprizio, M. P., Hamburg, S. P., and Jacob, D. J.: Satellite quantification
 971 of oil and natural gas methane emissions in the US and Canada including contributions from individual basins,
 972 *Atmospheric Chemistry and Physics*, 22, 11203–11215, <https://doi.org/10.5194/acp-22-11203-2022>, 2022.
- 973 Sherwin, E., Zhang, Z., Chen, Y., Wetherley, E. B., Yakovlev, P., Berman, E. S. F., Jones, B. B., Thorpe, A. K.,
 974 Ayasse, A. K., Duren, R., Brandt, A. R., and Cusworth, D. H.: Quantifying oil and natural gas system emissions using
 975 one million aerial site measurements, <https://doi.org/10.21203/rs.3.rs-2406848/v1>, 2023a.
- 976 Sherwin, E. D., Rutherford, J. S., Chen, Y., Aminfard, S., Kort, E. A., Jackson, R. B., and Brandt, A. R.: Single-blind
 977 validation of space-based point-source detection and quantification of onshore methane emissions, *Sci Rep*, 13, 3836,
 978 <https://doi.org/10.1038/s41598-023-30761-2>, 2023b.
- 979 Sherwin, E. D., Rutherford, J. S., Zhang, Z., Chen, Y., Wetherley, E. B., Yakovlev, P. V., Berman, E. S. F., Jones, B.
 980 B., Cusworth, D. H., Thorpe, A. K., Ayasse, A. K., Duren, R. M., and Brandt, A. R.: US oil and gas system emissions
 981 from nearly one million aerial site measurements, *Nature*, 627, 328–334, [https://doi.org/10.1038/s41586-024-07117-](https://doi.org/10.1038/s41586-024-07117-5)
 982 5, 2024.
- 983 Stavropoulou, F., Vinković, K., Kers, B., de Vries, M., van Heuven, S., Korbeń, P., Schmidt, M., Wietzel, J., Jagoda,
 984 P., Necki, J. M., Bartyzel, J., Maazallahi, H., Menoud, M., van der Veen, C., Walter, S., Tuzson, B., Ravelid, J.,
 985 Morales, R. P., Emmenegger, L., Brunner, D., Steiner, M., Hensen, A., Velzeboer, I., van den Bulk, P., Denier van
 986 der Gon, H., Delre, A., Edjabou, M. E., Scheutz, C., Corbu, M., Iancu, S., Moaca, D., Scarlat, A., Tudor, A., Vizireanu,
 987 I., Calcan, A., Ardelean, M., Ghemulet, S., Pana, A., Constantinescu, A., Cusa, L., Nica, A., Baciuc, C., Pop, C.,
 988 Radovici, A., Mereuta, A., Stefanie, H., Dandocsi, A., Hermans, B., Schwietzke, S., Zavala-Araiza, D., Chen, H., and
 989 Röckmann, T.: High potential for CH₄ emission mitigation from oil infrastructure in one of EU’s major production
 990 regions, *Atmospheric Chemistry and Physics*, 23, 10399–10412, <https://doi.org/10.5194/acp-23-10399-2023>, 2023.
- 991 Thorpe, M. J., Krieting, A., Altamura, D., Dudiak, C. D., Conrad, B. M., Tyner, D. R., Johnson, M. R., Brasseur, J.
 992 K., Roos, P., Kunkel, W., Carre-Burritt, A., Abate, J., Price, T., Yeralian, D., Kennedy, B., Newton, E., Rodriguez,
 993 E., Elfar, O. I., and Zimmerle, D. J.: Deployment-invariant probability of detection characterization for aerial LiDAR
 994 methane detection, 2024.
- 995 Tyner, D. R. and Johnson, M. R.: Where the Methane Is—Insights from Novel Airborne LiDAR Measurements
 996 Combined with Ground Survey Data, *Environ. Sci. Technol.*, 55, 9773–9783, <https://doi.org/10.1021/acs.est.1c01572>,
 997 2021.
- 998 Inventory of U.S. Greenhouse Gas Emissions and Sinks: [https://www.epa.gov/ghgemissions/inventory-us-](https://www.epa.gov/ghgemissions/inventory-us-greenhouse-gas-emissions-and-sinks)
 999 [greenhouse-gas-emissions-and-sinks](https://www.epa.gov/ghgemissions/inventory-us-greenhouse-gas-emissions-and-sinks), last access: 6 March 2024.
- 1000 EPA’s Final Rule for Oil and Natural Gas Operations Will Sharply Reduce Methane and Other Harmful Pollution.:
 1001 <https://www.epa.gov/controlling-air-pollution-oil-and-natural-gas-operations/epas-final-rule-oil-and-natural-gas>, last
 1002 access: 5 March 2024.
- 1003 Weller, Z. D., Hamburg, S. P., and von Fischer, J. C.: A National Estimate of Methane Leakage from Pipeline Mains
 1004 in Natural Gas Local Distribution Systems, *Environ. Sci. Technol.*, 54, 8958–8967,
 1005 <https://doi.org/10.1021/acs.est.0c00437>, 2020.
- 1006 Williams, J. P., Regehr, A., and Kang, M.: Methane Emissions from Abandoned Oil and Gas Wells in Canada and the
 1007 United States, *Environ. Sci. Technol.*, 55, 563–570, <https://doi.org/10.1021/acs.est.0c04265>, 2021.

1008 Williams, J. P., El Hachem, K., and Kang, M.: Controlled-release testing of the static chamber methodology for direct
1009 measurements of methane emissions, *Atmospheric Measurement Techniques*, 16, 3421–3435,
1010 <https://doi.org/10.5194/amt-16-3421-2023>, 2023.

1011 Worden, J. R., Cusworth, D. H., Qu, Z., Yin, Y., Zhang, Y., Bloom, A. A., Ma, S., Byrne, B. K., Scarpelli, T.,
1012 Maasackers, J. D., Crisp, D., Duren, R., and Jacob, D. J.: The 2019 methane budget and uncertainties at 1° resolution
1013 and each country through Bayesian integration Of GOSAT total column methane data and a priori inventory estimates,
1014 *Atmospheric Chemistry and Physics*, 22, 6811–6841, <https://doi.org/10.5194/acp-22-6811-2022>, 2022.

1015 Xia, H., Strayer, A., and Ravikumar, A. P.: The Role of Emission Size Distribution on the Efficacy of New
1016 Technologies to Reduce Methane Emissions from the Oil and Gas Sector, *Environ. Sci. Technol.*, 58, 1088–1096,
1017 <https://doi.org/10.1021/acs.est.3c05245>, 2024.

1018 Yacovitch, T. I., Herndon, S. C., Pétron, G., Kofler, J., Lyon, D., Zahniser, M. S., and Kolb, C. E.: Mobile Laboratory
1019 Observations of Methane Emissions in the Barnett Shale Region, *Environ. Sci. Technol.*, 49, 7889–7895,
1020 <https://doi.org/10.1021/es506352j>, 2015.

1021 Zhang, Y., Gautam, R., Pandey, S., Omara, M., Maasackers, J. D., Sadavarte, P., Lyon, D., Nesser, H., Sulprizio, M.
1022 P., Varon, D. J., Zhang, R., Houweling, S., Zavala-Araiza, D., Alvarez, R. A., Lorente, A., Hamburg, S. P., Aben, I.,
1023 and Jacob, D. J.: Quantifying methane emissions from the largest oil-producing basin in the United States from space,
1024 *Science Advances*, 6, eaaz5120, <https://doi.org/10.1126/sciadv.aaz5120>, 2020.

1025 Zhou, X., Yoon, S., Mara, S., Falk, M., Kuwayama, T., Tran, T., Cheadle, L., Nyarady, J., Croes, B., Scheehle, E.,
1026 Herner, J. D., and Vijayan, A.: Mobile sampling of methane emissions from natural gas well pads in California,
1027 *Atmospheric Environment*, 244, 117930, <https://doi.org/10.1016/j.atmosenv.2020.117930>, 2021.

1028 Zimmerle, D., Vaughn, T., Luck, B., Lauderdale, T., Keen, K., Harrison, M., Marchese, A., Williams, L., and Allen,
1029 D.: Methane Emissions from Gathering Compressor Stations in the U.S., *Environ. Sci. Technol.*, 54, 7552–7561,
1030 <https://doi.org/10.1021/acs.est.0c00516>, 2020.

1031

1032

1033

1034

1035

1036

1037

